TAMPERE UNIVERSITY OF TECHNOLOGY

TIIA TIKKANEN

# Computer Simulations of Scanning Tunneling Microscopy of Adsorbate Molecules on Metal Surfaces

Master of Science Thesis

Examiners: Doc. Jouko Nieminen,
Prof. Adam Foster
The subject was approved by the
Department Council meeting
4.4.2012

# TIIVISTELMÄ

TAMPEREEN TEKNILLINEN YLIOPISTO
Teknis-luonnontieteellinen koulutusohjelma
**TIKKANEN, TIIA: Metallipinnalle adsorboituneiden molekyylien pyyhkäisytunnelointimikroskopian tietokonesimulaatioita**
Diplomityö, 50 sivua, 15 liitesivua
Heinäkuu 2012
Pääaine: Teknillinen fysiikka
Tarkastajat: Dos. Jouko Nieminen, Prof. Adam Foster
Avainsanat: tunnelointi, pyyhkäisytunnelointimikroskopia, STM, adsorbaatti, metallipinnat, GPAW, epätasapainon Greenin funktiot, NEGF

Pyyhkäisytunnelointimikroskopia (eng. Scanning tunneling microscopy, STM) on yksi modernin pintatieteen tärkeimmistä työkaluista. Se mahdollistaa atomirakenteen kuvantamisen reaaliavaruudessa ja pintojen tutkimisen atomimittakaavassa. Menetelmä perustuu kvanttimekaaniseen tunneloitumiseen, jonka ansiosta paikallisen kärjen ja tutkittavan pinnan välille syntyy virta. Kun kärkeä liikuttamalla käydään koko pinta läpi, saadaan topografinen kuva, joka antaa tietoa pinnasta atomitasolla.

Kokeelliset tulokset metallipinnalle adsorboituneiden molekyylien pyyhkäisytunnelointimikroskopiasta ovat osoittaneet, että saatu topografinen kuva ei välttämättä vastaa tutkitun systeemin geometrista rakennetta. Siksi kokeellisten STM-kuvien ymmärtämisessä ja tulkitsemisessa STM:n teoreettinen ja laskennallinen mallintaminen on oleellista.

Tämä diplomityö keskittyy metallipinnalle adsorboituneiden molekyylien pyyhkäisytunnelointimikroskopian mallintamiseen. Tavoitteena on testata GPAW-ohjelmiston toimivuutta mallinnuksessa. Simulaatioissa tutkitaan, miten adsorbaattimolekyylin lisääminen metallipinnalle vaikuttaa STM-kuviin. Tämä tehdään simuloimalla sekä puhdasta metallipintaa että pintaa, jolle on adsorboitunut molekyyli. Lisäksi työssä simuloidaan elektronien transmissiota molekyylien läpi, jotta adsorbaattimolekyylien vaikutus elektronien tunneloitumiseen saadaan selville.

STM-kuvat saadaan puhtaalle Al(111)-pinnalle ja pinnalle, jolle $O_2$ molekyyli on adsorboitunut. Kuvissa adsorbaattimolekyyli nähdään pinnalla painaumana eikä kohoumana kuten geometrisen rakenteen perusteella oletettaisiin. Kuvat näyttävät, että adsorbaattimolekyylin lisääminen vaikuttaa laajasti koko STM-kuvaan. Transmissiosimulaatiot eri molekyylien läpi osoittavat molekyylin elektronirakenteen vaikuttavan elektronien tunneloitumiseen. GPAW:n STM-simulaatiopaketin todetaan toimivan vain tiettyjen systeemien STM-simuloinnissa.

# ABSTRACT

TAMPERE UNIVERSITY OF TECHNOLOGY
Master's Degree Programme in Science and Engineering
**TIKKANEN, TIIA: Computer Simulations of Scanning Tunneling Microscopy of Adsorbate Molecules on Metal Surfaces**
Master of Science Thesis, 50 pages, 15 Appendix pages
July 2012
Major: Advanced Engineering Physics
Examiners: Doc. Jouko Nieminen, Prof. Adam Foster
Keywords: tunneling, scanning tunneling microscopy, STM, adsorbates, metal surfaces, grid-based projector augmented wave method, GPAW, non equilibrium Green's functions, NEGF

Scanning tunneling microscopy is one of the most important tools in modern surface science. It enables imaging of the atomic structure in real space and exploration of surfaces in atomic scale. It is based on quantum mechanical tunneling due to which a current arises between a local tip and a sample surface. Scanning the tip over the sample produces a topographic image, which provides information of the surface in atomic scale.

Experimental studies of scanning tunneling microscopy of adsorbate molecules on metal surfaces have proven that the measured topographic image might not resemble the geometrical structure of the researched system. Thus for understanding and interpretation of the experimental STM images, theoretical and computational modeling of scanning tunneling microscopy is essential.

This thesis concentrates on simulation of scanning tunneling microscopy of adsorbate molecules on metal surfaces. A main objective is to test the functionality of GPAW program package in the simulations. Simulations study the effect of an adsorbate on STM images. This is done by simulating both a clean surface and one with an adsorbate. In addition electron transport through molecules is simulated to see how transmission depends on adsorbate molecules.

STM images are received for both clean aluminium Al(111) surface and a surface with $O_2$ adsorbate. In the images the adsorbate molecule is seen as a depression on the surface rather than a protrusion as would be expected. The images show that the influence of the adsorbate molecule is wide. Transmission simulations through different molecules demonstrate that the electronic structure of the molecule affects tunneling of electrons. The GPAW's STM simulation package is discovered to only work with certain systems.

# PREFACE

I started working in the computational physics group in June 2011 and started immediately simulating scanning tunneling microscope systems with GPAW program package. We started off well, but calculating actual STM images proved to be problematic. Despite the problems and numerous different inconsistent error messages, the simulations were carried on and the problems were tried to solve. Finally, some successful STM images were received, and I am proud to present them in this thesis.

I want to thank my supervisor Jouko Nieminen for significant help with understanding the theory, help with simulation work, and for good comments during the writing process. Jouko was always encouraging and kept me going. Adam Foster should not be left unmentioned as without him the project would not have been possible. I also want to thank co-worker Mikael Kuisma for enormous help with GPAW and other problems I ran into. If it was not for his help, I would still be struggling with the simulations.

Finally, I want to thank all my friends for their support and for giving me time off from the thesis. Special thanks go to my family, who were left too little time with their dear Tiia. To myself I want to say: Tiia, you did it!

Tampere, 31th of July, 2012

Tiia Karoliina Tikkanen

# CONTENTS

# TERMS AND SYMBOLS

| | |
|---|---|
| AFM | Atomic Force Microscope/Microscopy |
| ASE | Atomic Simulation Environment |
| DFT | Density Functional Theory |
| DOS | Density Of States |
| EMT | Effective Medium Theory |
| FCC | Face Centered Cubic lattice structure |
| GPAW | Grid-based Projector Augmented Wave method |
| LCAO | Linear Combination of Atomic Orbitals |
| LDOS | Local Density Of States |
| PAW | Projector Augmented Wave method |
| PDOS | Projected Density Of States |
| SNOM | Scanning Near-field Optical Microscope/Microscopy |
| SPM | Scanning Probe Microscope/Microscopy |
| STM | Scanning Tunneling Microscope/Microscopy |
| STS | Scanning Tunneling Spectroscopy |

| | |
|---|---|
| a.u. | Arbitrary units |
| $\alpha$ | Isolated region |
| $A$ | Perturbation term |
| $A_n$ | Linear combination coefficient for perturbation term, $A$ |
| $A_{mn}$ | Perturbation matrix |
| $c_n$ | Linear combination coefficient |
| $d$ | Distance from STM tip to STM surface |
| $\delta$ | Dirac delta function |
| $\epsilon_n$ | Energy of the single particle wave function $\|\psi_n\rangle$ |
| $e$ | Elementary charge |
| $e$ | Exponential function |
| $E$ | Energy variable |
| $E_n$ | Energy of region $n$ |
| $E_F$ | Fermi energy |
| $f(E)$ | Fermi function |
| $f_{\mathsf{max}}$ | Maximum force on individual atom in structure |
| $\vec{F}_a$ | Force on an individual atom $a$ |
| $G$ | Green's function |
| $G^+$ | Retarded Green's function |
| $G^-$ | Advanced Green's function |
| $g_I$ | Green's function of an isolated region $I$ |

| | |
|---|---|
| $\Gamma_j$ | $i(\Sigma_j - \Sigma_j^\dagger)$ |
| $h$ | Planck's constant |
| $h$ | Grid spacing in GPAW |
| $H$ | Hamiltonian operator |
| $H_n$ | Hamiltonian of region n |
| $\tilde{H}$ | Hamiltonian in projector augmented wave method |
| $\Delta H_{ij}^a$ | Atomic Hamiltonian |
| $\hbar$ | $h/2\pi$ |
| $I$ | Tunneling current |
| $I, J$ | As a subscript denotes an isolated region |
| $i$ | Imaginary unit $\sqrt{-1}$ |
| $\Im(G)$ | Imaginary part of $G$ |
| $i\eta$ | Infinitesimal imaginary energy |
| $\mathbf{k}$ | $\mathbf{k}$-point |
| $\kappa$ | $\sqrt{(2m\phi/\hbar^2)}$ |
| $k_B$ | Boltzmann constant |
| $\mathcal{L}$ | Linear differential operator |
| $m$ | Electron mass |
| $\langle m\|$ | "Bra"-vector, dual of the $m$th member of a basis, which spans the Hilbert space |
| $M_{IJ}$ | Tunneling matrix element between regions $I$ and $J$ |
| $\mu$ | Chemical potential |
| $n$ | Subscript used to represent different eigenfunctions |
| $n, \ell, m$ | Principal, angular momentum and magnetic quantum numbers |
| $\|n\rangle$ | "Ket"-vector, $n$th member of a basis, which spans the Hilbert space, corresponds to the eigenfunction $\phi_n$ |
| $\eta$ | Infinitesimal convergence factor |
| $\tilde{p}_i^a$ | Smooth projector function of atom $a$ |
| $\mathbf{r}$ | Position vector |
| $\bar{r}$ | Position vector |
| $R$ | Radius of curvature of Tersoff-Hamann tip |
| $\bar{R}^a$ | Position of atom $a$ |
| $\mathbf{R}$ | Bravais vector |
| $\mathbf{r}_0$ | Center of curvature of Tersoff-Hamann tip |
| $r_c$ | Cutoff radius of atom $a$'s augmentation sphere |
| $R_{n\ell}^a$ | Radial function |
| $\rho$ | Density of states |
| $\rho^0$ | Density of states of the unperturbed system |
| $\rho(\mathbf{r}, E)$ | Local density of states |

| | |
|---|---|
| $\sigma$ | Conductance |
| $\Sigma_I$ | Self-energy |
| $S$ | Overlap operator |
| $S$ | Overlap matrix |
| $\vec{S}$ | Any surface separating two regions |
| $\Delta S_{ij}^a$ | Atomic overlap operator |
| $t$ | Time |
| $T$ | Temperature |
| $\tau$ | Overlap of wave functions of different regions |
| $\hat{T}$ | Linear transformation operator |
| $\hat{T}^a$ | Linear transformation operator of atom $a$ |
| $T_{IJ}$ | Transition matrix between regions $I$ and $J$ |
| $V$ | Bias voltage |
| $V$ | Perturbation potential |
| $V_{IJ}$ | Coupling between regions $I$ and $J$ |
| $\tilde{v}$ | Effective potential |
| $x, y, z$ | Cartesian coordinates |
| $Y_{\ell m}$ | Spherical harmonic |
| $\phi$ | Work function |
| $\phi_i$ | Wave function of region $i$ |
| $\phi_i^a$ | Partial wave function of atom $a$ |
| $\tilde{\phi}_i^a$ | Smooth partial wave function of atom $a$ |
| $\varphi_n$ | $n$th eigenfunction |
| $\psi_i$ | Wave function of region $i$ |
| $\|\psi_n\rangle$ | Single particle wave function |
| $\|\tilde{\psi}_n\rangle$ | Smooth pseudo wave function |

# 1. INTRODUCTION

Scanning tunneling microscopy (STM) was discovered three decades ago by Binnig and Rohrer [1]. The discovery was groundbreaking, as it, for the first time, enabled imaging of the atomic structure in real space. Since the 1980's STM has been of tremendous help in surface exploration in atomic scale, and to this day it has kept its position in being one of the most important tools in modern surface science. The inventors of STM were awarded the Nobel Prize in 1986 for development of the STM technique. [2]

In STM a fine needlelike electrically conductive tip is scanned a few Ångströms above a sample surface to produce a topographic surface image. The method is based on the tunneling phenomenon, which allows electrons to cross the potential barrier between tip and surface when a bias voltage is added to the system. Tunneling of electrons produces a current, which depends on the distance between tip and surface. If the tunneling current is kept constant as the tip is scanned through the surface, the tip height is forced to change, and therefore an image of the surface's geometric structure is obtained. [2]

Figure 1.1 illustrates the experimental STM setup. The principle of operation of STM is as follows. To control the position of the STM tip, it is attached to a piezoelectric tube. Depending on the voltage applied to the tube its piezoelectric crystals expand or contract very slightly and the tip's distance from surface is changed. Distance control and scanning unit applies the voltage to the tube and thus controls the tip movement. As the tip is brought close to the STM sample surface with an added voltage, a tunneling current arises. The tunneling current is conducted through a tunneling current amplifier to the distance control unit. If the current is too large or too small, the distance control moves the tip height until the preset current is reached. The movement of the tip is recorded and displayed on a screen. As the tip is scanned over the surface, a map of the surface topography is received. [3, 4]

The impulse towards STM arose from the need for study of metal surfaces in the atomic scale. The interest was especially on materials used in miniature electronic devices. For this local study of the surface, an idea of using vacuum tunneling arose. The idea was old in principle, but it had not been explored with devotion earlier. [6] The discovery of STM was, therefore, the realization that this kind of local probing

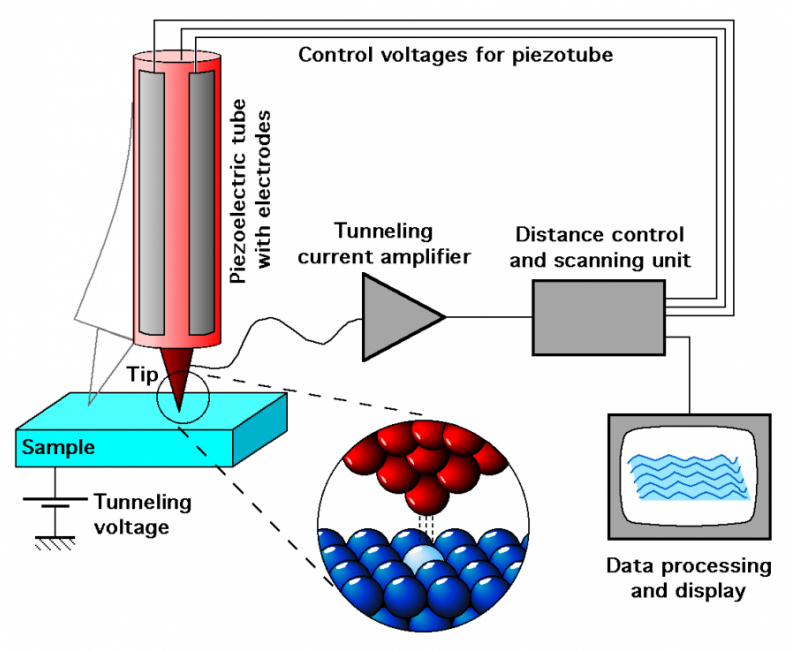


Figure 1.1: A schematic view of the setup of scanning tunneling microscope. [5]

with a tip is possible [7].

The development in STM soon generated other local-probe methods, when attention was drawn to other type of interactions that arose due to the presence or touch of a local probe. Scanning near-field optical microscope, SNOM [8], and atomic force microscope, AFM [9], were the first followers. In SNOM the photon current is the measure of the interaction, and in AFM different forces are studied. The invention of AFM was a major extension to local-probe methods, as it allowed imaging of both conducting and nonconducting objects. [7] Following these methods, a whole family of scanning probe microscopies, SPM, appeared, each of which make use of different interactions and different properties of the surface in different environments [2, 7]. Applications exist for electronic and vibrational properties [10, 11], film growth [12, 13], measurement of adhesion and strength of individual chemical bonds [14, 15, 16], studies of friction and lubrication [17, 18, 19], dielectric and magnetic properties [20, 21], molecular manipulation [22, 23], and many other phenomena from micrometer to subnanometer scale. [24]

A particularly interesting application is the local manipulation and modification of the surface with a local-probe. Interactions between surface and probe are observed to give rise to breaking of individual chemical bonds and to initiating local chemical reactions. The local deformations can be reversible or irreversible. [7] The irreversible deformation forms a basis to atom manipulation [22]. The chance of an deformation is to be noted in experiments, as in imaging the irreversible deformations are unwanted. To avoid these features, extreme accuracy is essential.

[7]

In addition to local-probe methods, STM was early on generalized to scanning tunneling spectroscopy, STS, where the tunneling current, $I$, is measured as a function of the bias voltage, $V$ [25]. In STS the tip is positioned at one point above the surface. This provides the differential conductance $\sigma = dI/dV$, which is very sensitive to surface electronic states, so measuring the differential conductance enables probing the local density of states, LDOS, of the sample. [26]

Experimenting with scanning tunneling microscope has taught that the image obtained does not necessarily correspond to the actual geometric structure of the sample, as the tunneling current depends also on the electronic structure of the sample. An adsorbate on a sample surface might be seen on the STM image as a depression rather than a protrusion even though the adsorbate is geometrically higher than the surface [27]. The unpredictability of the experimental STM images proves a need for theoretical modeling of scanning tunneling microscope. Theoretical models and simulation is needed to provide understanding of the experimental results and to interpret the peculiar images obtained. [28]

The theory of STM focuses on calculation of the tunneling current between the tip and surface, for which several methods have been developed over the years [29]. One of the main approaches is the Bardeen's approach [30] that was developed prior to the actual scanning tunneling microscope. As applied to STM, the method treats STM tip and surface as separate entities, and concludes that the tunneling current can be derived from the overlap of the tip and surface's wave functions. Other main approaches are the Tersoff Hamann approach [31], the scattering approach [32] and non equilibrium Green's functions approach [33].

Although theories developed for scanning tunneling microscope have been available for many decades, there are few softwares that concentrate on STM simulations. A new simulation software is the commercial Nt_STM [34], which enables easy building of realistic STM systems, simulating topographic images as well as I(V) spectra, and other various properties interesting in STM. In this thesis the simulations are done using the grid-based projector augmented wave, GPAW, method that includes ready codes for Bardeen type STM simulations using non equilibrium Green's functions.

The aim of this thesis is to demonstrate the useability of the grid-based projector augmented wave method in Bardeen type STM calculations of surfaces with adsorbates. The main interest is in comparing the calculated results to experimental STM images of the same system. In addition electron transport calculations are carried out. Electron transport calculations give the transmission coefficient of the electrons, which is proportional to the conductance, and thus it can be used in modeling STS. The calculations are carried out in the atomic orbital basis set using

non equilibrium Green's functions. Simulations are done to Cu(111) and Al(111) surfaces with and without adsorbate molecules $O_2$ and $H_2$.

The structure of this thesis is as follows. Chapter 2 introduces the theory behind the simulations. First off tunneling phenomenon and Bardeen's approach to solving the tunneling current is presented, and then the important Green's functions and non equilibrium Green's functions are visited. The STM theory is finally introduced using the approach of Todorov and Pendry [35, 36]. Chapter 3 presents the used simulation methods and GPAW, and in chapter 4 the simulated systems and the results of the simulations are presented. Final chapter 5 is discussion and conclusions.

# 2. THEORY

Scanning tunneling microscope, STM, was introduced by Binnig and Rohrer in 1981 [1]. The method introduced was very simple: In STM a fine needlelike electrically conductive tip is scanned a few Ångströms above a sample surface. When a small voltage is added to the tip, electrons tunnel between the surface and tip, and a current arises due to quantum mechanical tunneling. [37] The current changes as the tip is moved on the surface. Keeping the distance or current between tip and surface constant, the current or distance changes respectively. These are called the constant height and constant current modes. As the tip is scanned over the surface, topographic images are received and features of the surface can be derived. [2]

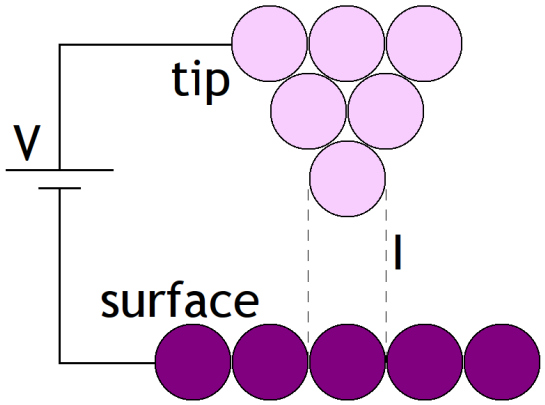


Figure 2.1: Model picture of the STM tip and STM sample surface. When a bias voltage $V$ is added, a current, $I$, arises between tip and surface.

This chapter is dedicated to the theory behind the work done in this thesis. Before presenting theory of actual scanning tunneling microscope as derived by Todorov and Pendry [35, 36], the tunneling phenomenon is considered, and Green's functions and non equilibrium Green's functions are briefly introduced. The theory section is rather short but sufficient to present the main theory behind the calculations.

## 2.1 Tunneling

Scanning tunneling microscope is based on quantum mechanical tunneling. In tunneling a particle tunnels through a barrier that it classically could not cross. In scanning tunneling microscope the gap between tip and surface forms a potential

barrier. Thanks to the tunneling phenomenon, electrons are allowed to pass through the barrier and thus a current may arise.

When no bias voltage is present, the amount of electrons to travel from tip to surface is the same as the amount of electrons traveling from surface to tip. Applying a positive bias voltage lowers the Fermi surface on the lower potentials side. Now the tunneling occurs from the occupied states to the unoccupied states. [6] The applied bias voltage in STM is typically between 1 mV and 4 V, which induces a current in the range from 10 pA to 10 nA [2]. In picture 2.2 the electron tunneling through a barrier is demonstrated with and without an added bias voltage.

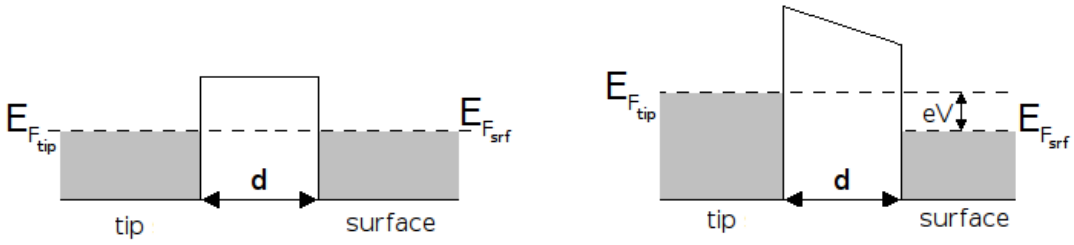


Figure 2.2: One-dimensional model picture of tunneling through a barrier of width $d$ without and with a bias voltage $V$. A positive bias voltage added to the surface region shifts the energies down by $eV$. $E_{F_{\text{tip}}}$ and $E_{F_{\text{srf}}}$ denote the Fermi levels of tip and surface, respectively.

If the tunneling problem is treated as a one-dimensional problem, the tunneling current through a barrier of width $d$ is written

$$I \propto e^{-2\kappa d}. \tag{2.1}$$

Here $\kappa = \sqrt{\frac{2m\phi}{\hbar^2}}$, where $m$ is the electron mass, $\hbar = h/2\pi$ and $\phi$ denotes the work function of the tunneling electron. [38] The values of work functions of different metals are around 5 eV [39]. The formula reveals the sensitivity of the tunneling current to the variation of the distance $d$: as the distance between tip and surface is increased by an Ångström, the change in the tunneling current is tenfold. However, to receive a better approximation of the tunneling current and understanding of the problem, the tridimensionality and electronic structure of the tip and surface must be noted.

In Bardeen's formalism [30] the tunneling problem is approached by separating the system to two distinct subsystems, region 1 and 2, for which the Hamiltonians, $H_1$ and $H_2$, wave functions, $\psi_1$ and $\psi_2$, and corresponding energies in the absence of tunneling, $E_1$ and $E_2$, are known. The tunneling current between these regions

depends on the overlap of their wave functions, that is, orbitals.

$$I = \frac{2\pi e}{\hbar} \sum_{1,2} f(E_1)[1 - f(E_2 + eV)]|M_{12}|^2 \delta(E_1 - E_2). \tag{2.2}$$

Here $V$ is the applied bias voltage, $\delta$ is the Dirac delta function and $f(E)$ is the Fermi function

$$f(E) = \frac{1}{e^{(E-\mu)/k_B T} + 1}, \tag{2.3}$$

where $\mu$ is the chemical potential and $T$ is temperature. $M_{12}$ in equation 2.2 is the tunneling matrix element between states $\psi_1$ and $\psi_2$:

$$M_{12} = \frac{\hbar^2}{2m} \int d\vec{S}(\psi_1^* \nabla \psi_2 - \psi_2 \nabla \psi_1^*). \tag{2.4}$$

The integral is over any surface $\vec{S}$ in the barrier region separating regions 1 and 2. [30]

To achieve the tunneling current, evaluation of the tunneling matrix must be done. Further evaluation of the matrix element $M$ was done by Tersoff and Hamann. They modeled the tip as a locally spherical potential well and the surface wave function as a Bloch wave function to achieve a definition to $M$. The STM system is illustrated in picture 2.3. This kind of approximation lead to a result that the tunneling current is actually proportional to the local density of states (LDOS), $\rho(\mathbf{r}_0, E_F)$, of the surface at the Fermi level of the tip. [31]

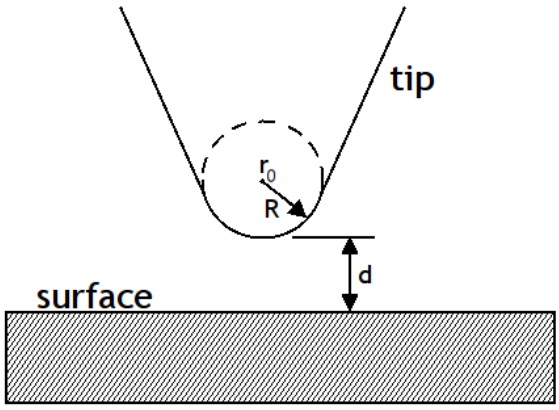


Figure 2.3: Schematic picture of Tersoff-Hamann model tip and surface. Tip is assumed locally spherical with radius of curvature $\mathbf{R}$, the center of curvature being $\mathbf{r}_0$. $d$ is the distance to the surface.

$$I \propto \sum_1 |\psi_1(\mathbf{r}_0)|^2 \delta(E_1 - E_F) \equiv \rho(\mathbf{r}_0, E_F) \tag{2.5}$$

This means that at constant current the tip follows a contour of constant local

density of states and actually the STM image is a contour of LDOS of the surface at Fermi level. So, to understand the tunneling current, examination of the local density of states is important.

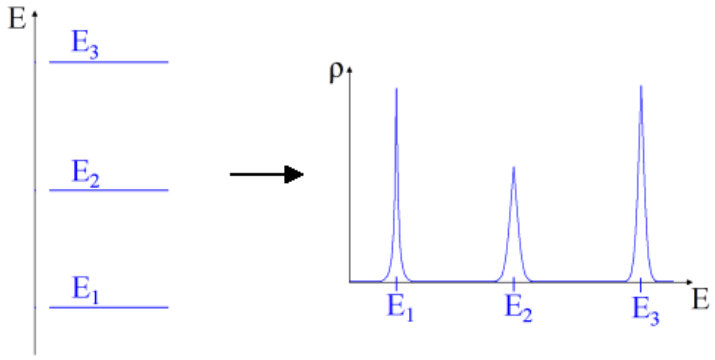


Figure 2.4: The connection between density of states and the energy distribution.

The density of states can be written as a sum of separate density of states for each eigenstate, which are delta function's peaks (see picture 2.4):

$$\rho = \sum_i \rho_i(E) = \sum_i \delta(E - E_i), [40] \tag{2.6}$$

so actually the density of states is found already in Bardeen's tunneling current formula 2.2 for energy $E_1$.

Density of states has a connection to the imaginary part of a Green's function, $\Im(G(E))$, as follows:

$$-\frac{1}{\pi}\Im(G(E+i\eta)) = \frac{1}{E-H+i\eta} \xrightarrow{\eta\to 0} \delta(E-H). \tag{2.7}$$

That is: as the value of Green's function's imaginary part approaches zero, the formula approaches the delta function and hence the density of states

$$\rho = -\frac{1}{\pi}\Im(G(E+i\eta)).[41] \tag{2.8}$$

This finding leads to the next section, where Green's functions are introduced.

## 2.2 Green's functions

Before continuing to the theory of scanning tunneling microscope, a short introduction to Green's functions is given. As presented in the previous section, Green's functions can be used to calculate the density of states. In addition Green's functions are propagators and, therefore, they give the probability amplitude for a particle to

travel from one point to another in time $t$. Green's functions are also useable in perturbation theory, as they describe how a system reacts to a continuous perturbation. [42] Thus Green's functions are connected to scanning tunneling microscope from the viewpoint of DOS, and as propagators they give theoretical framework to tunneling calculations. Mathematically Green's function, $G$, is taken to be a solution of a linear inhomogeneous differential equation

$$\mathcal{L}G(\mathbf{r}_1, \mathbf{r}_2) = \delta(\mathbf{r}_1, \mathbf{r}_2), \tag{2.9}$$

where $\mathcal{L}$ is a linear differential operator and $\delta(\mathbf{r}_1, \mathbf{r}_2)$ is the Dirac delta function [43].

Let's consider an isolated unperturbed system, which is described by a discrete Schrödinger equation:

$$H\left|n\right\rangle = E\left|n\right\rangle \Leftrightarrow (E_n - H)\varphi_n(\mathbf{r}) = 0. \tag{2.10}$$

Here $H$ is the Hamiltonian, the operator corresponding to the total energy of the system. The solutions of the Schrödinger equation are the eigenvalues $\{E_n\}$ and the corresponding eigenfunctions $\{\varphi_n(r)\}$.

Summing over all the eigenfunctions gives

$$\sum_n \varphi_n^*(\mathbf{r})\varphi_n(\mathbf{r}') = \delta(\mathbf{r} - \mathbf{r}'), \tag{2.11}$$

where $\delta(\mathbf{r} - \mathbf{r}')$ is the Dirac delta function[1].

An arbitrary function $\psi(\mathbf{r})$ can be expressed as a linear combination of functions $\varphi_n(\mathbf{r})$

$$\psi(\mathbf{r}) = \sum_n c_n\varphi_n(\mathbf{r}). \tag{2.12}$$

The coefficients $c_n$ are

$$c_n = \int \varphi_n^*(\mathbf{r}')\psi(\mathbf{r}')d\mathbf{r}', \tag{2.13}$$

and so equation 2.12 can be re-evaluated:

$$\psi(\mathbf{r}) = \int \sum_n \varphi_n^*(\mathbf{r}')\varphi_n(\mathbf{r})\psi(\mathbf{r}')d\mathbf{r}' \Leftrightarrow \psi(\mathbf{r}) = \int \delta(\mathbf{r} - \mathbf{r}')\psi(\mathbf{r}')d\mathbf{r}'. \tag{2.14}$$

When a perturbation $V$ is added to the system, the Schrödinger is rewritten:

$$H\psi + V\psi = E\psi \Leftrightarrow (H + V)\psi = E\psi \Leftrightarrow (E - H)\psi = V\psi. \tag{2.15}$$

This is similar to a situation where an STM tip is moved close to the STM surface

[1] For Dirac delta function: $\int_{-\infty}^{\infty} f(x)\delta(x - x_0) = f(x_0)$. [44]

and causes a perturbation. The solutions of equation 2.15 are the wave functions $\psi(\mathbf{r})$, as in equation 2.12.

Now the perturbation term $V\psi$ is denoted by term $A = V\psi$ for which

$$A(\mathbf{r}) = \sum_n A_n \varphi_n(\mathbf{r}) = \int \sum_n \varphi_n^*(\mathbf{r}')\varphi_n(\mathbf{r})A(\mathbf{r}')d\mathbf{r}'. \tag{2.16}$$

Combining the equations 2.15 and 2.12 translates equation 2.15 further on to

$$\sum_n (E - H)\varphi_n(\mathbf{r})c_n = \sum_n (E - E_n)\varphi_n(\mathbf{r})c_n = \sum_n A_n\varphi_n(\mathbf{r}), \tag{2.17}$$

which ultimately leads to the coefficient value

$$c_n = \frac{A_n}{E - E_n}. \tag{2.18}$$

When $c_n$ is substituted to the original solution of the wave function, equation 2.12, the wave function is received in respect to a Green's function $G(\mathbf{r} - \mathbf{r}')$:

$$\psi(\mathbf{r}) = \sum_n \frac{A_n\varphi_n(\mathbf{r})}{E - E_n} = \int \sum_n \frac{\varphi_n^*(\mathbf{r}')\varphi_n(\mathbf{r})}{E - E_n} A(\mathbf{r}')d\mathbf{r}' = \int G(\mathbf{r} - \mathbf{r}')A(\mathbf{r}')d\mathbf{r}'. \tag{2.19}$$

The Green's matrix is derived. The perturbation $A$ can be written as a matrix:

$$A_{mn} = \int \varphi_m^*(\mathbf{r})A(\mathbf{r})\varphi_n(\mathbf{r})d\mathbf{r} = \langle m|A|n\rangle = \int \langle m|\mathbf{r}\rangle\, A(\mathbf{r})\, \langle \mathbf{r}|n\rangle\, d\mathbf{r}. \tag{2.20}$$

so the perturbation $A(\mathbf{r}, \mathbf{r}')$ is

$$A(\mathbf{r}, \mathbf{r}') = \sum_{mn} \langle \mathbf{r}|m\rangle\, A_{mn}\, \langle n|\mathbf{r}'\rangle = \sum_{mn} \varphi_n^*(\mathbf{r}')\varphi_n(\mathbf{r})A_{mn}. \tag{2.21}$$

The Green's function can similarly be written as

$$G(\mathbf{r} - \mathbf{r}') = \sum_{mn} \varphi_n^*(\mathbf{r}')\varphi_m(\mathbf{r})G_{mn}, \tag{2.22}$$

where $G_{mn}$ is the Green's matrix:

$$G_{mn} = \frac{\delta_{mn}}{E - E_n}. \tag{2.23}$$

Here $\delta_{mn}$ denotes the Kroenecker delta function.

$E - H$ can be expressed as a matrix $\langle m|(E - H)|n\rangle = (E - E_n)\delta_{mn}$. The inverse

of the matrix is defined:

$$[(E-H)^{-1}]_{mn} = \frac{\delta_{mn}}{E-E_n} = G_{mn}. \tag{2.24}$$

Thus the definition of Green's function can be written:

$$G = (E-H)^{-1} \Leftrightarrow (E-H)G(E) = I. \tag{2.25}$$

If the energy $E$ is increased or decreased by an infinitesimal term $i\eta \to 0$, the retarded (causal) and advanced Green's functions, $G^+$ and $G^-$, are received:

$$G^{\pm}(E+i\eta) = \frac{1}{E-H\pm i\eta}. \tag{2.26}$$

Physically these Green's functions represent the causality of the propagation. In the retarded scheme the perturbation follows the movement of a particle, whereas in the advanced scheme the perturbation precedes the particle's movement. Retarded Green's function defines the propagation of the electron to a empty space (hole) and advanced Green's function the propagation of the hole to the site of an electron (see picture 2.5). Later it is seen that the convergence factor $\eta$ has a connection to the environment of the electron system, which can be taken into account with a self-energy term.

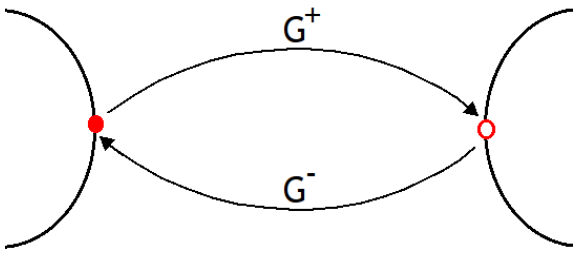


Figure 2.5: The retarded Green's function $G^+$ defines the movement of a particle to a empty state whereas the advanced Green's function $G^-$ moves the hole to an occupated site.

Green's functions can be used to describe how a system reacts to a continuous perturbation $A = V\psi$. When the Green's function of the system is known, the wave function under continuous perturbation can be simply derived from equation 2.15

$$\psi = \psi^0 + (E-H)^{-1}A = \psi^0 + GA = \psi^0 + GV\psi, \tag{2.27}$$

where $(E-H)\psi^0 = 0$ (the unperturbed situation), $\psi^0$ is the unperturbed wave function and $V$ is the potential of the perturbation. The last form of the equation

2.27 is the general form of the Lippmann-Schwinger [45]:

$$\psi = \psi^0 + G^0 V\psi \Rightarrow (I - G^0 V)\psi = \psi^0 \Rightarrow \psi = \psi^0 + G^0 V(1 - G^0 V)^{-1}\psi^0. \quad (2.28)$$

Substituting $T = V(I - G^0 V)^{-1}$ the following form is received:

$$\psi = \psi^0 + G^0 T\psi^0. \quad (2.29)$$

This implies that to obtain the wave function in the perturbed scheme, only the unperturbed Green's function, $G^0$, unperturbed wave function, $\psi^0$, and the perturbation $V$ must be known.

### 2.2.1 Non equilibrium Green's functions

Transport systems are formed of two leads that trap between them a nanostructure. When there is a potential difference between the leads, current arises between them and flows through the nanostructure. The system is then regarded to be in non equilibrium. [46] To study non equilibrium systems, non equilibrium Green's function (NEGF) formalism (Keldysh or the Kadanoff-Baym [47] formalism) is introduced. It is an extremely useful tool in studying non equilibrium many-particle systems and widely used to describe transport phenomena. This section is an easy-going introduction to non equilibrium Green's functions, which follows the Paulsson's paper [48] on the subject.

In NEGF formalism the system is divided into two contacts $1, 2$ and a device $d$ between them (see picture 2.6). System can for instance consist of a molecule and two surrounding leads. As the subsystems are thought of as separate systems, they have their own Hamiltonians and corresponding wave functions: $H_1$, $H_2$, $H_d$ and $\psi_1$, $\psi_2$, $\psi_d$.

$$\begin{aligned} H_1 |\psi_1\rangle &= E_1 |\psi_1\rangle \\ H_d |\psi_d\rangle &= E_d |\psi_d\rangle \\ H_2 |\psi_2\rangle &= E_2 |\psi_2\rangle \end{aligned} \quad (2.30)$$

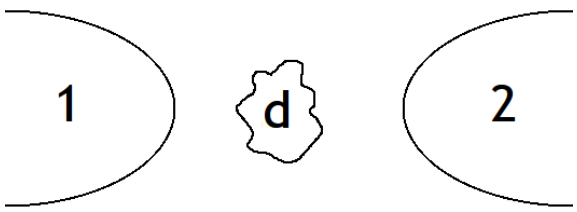


Figure 2.6: Division of the NEGF system to device $d$, and contacts 1 and 2 around them.

When the subsystems are close to each other, a connection arises between them.

The total Hamiltonian of the system can be then written as a tridimensional matrix and the discrete Schrödinger equation is written

$$H|n\rangle = E|n\rangle \Rightarrow \begin{pmatrix} H_1 & \tau_1 & 0 \\ \tau_1^\dagger & H_d & \tau_2^\dagger \\ 0 & \tau_2 & H_2 \end{pmatrix} \begin{pmatrix} |\psi_1\rangle \\ |\psi_d\rangle \\ |\psi_2\rangle \end{pmatrix}, \tag{2.31}$$

where $\tau_i$ describes the interaction between device and contact, that is, how intensively the wave functions of the device and contact overlap

$$\tau_i = \int \psi_d^* H \psi_i d^3\mathbf{r} = \langle \psi_d | H | \psi_i \rangle \tag{2.32}$$

and $\tau_i^\dagger$ is its conjugate transpose

$$\tau_i^\dagger = \langle \psi_i | H | \psi_d \rangle . \tag{2.33}$$

Between the two contacts, 1 and 2, no interaction is met.

With the help of Green's functions, the wave function of the contact $|\psi_2\rangle$ can be calculated from equation 2.31's third row:

$$\begin{aligned} 0|\psi_1\rangle + \tau_2|\psi_d\rangle + H_2|\psi_2\rangle &= E|\psi_2\rangle \\ \Leftrightarrow (E - H_2)|\psi_2\rangle &= \tau_2|\psi_d\rangle \\ |\psi_2\rangle &= g_2(E)\tau_2|\psi_d\rangle , \end{aligned} \tag{2.34}$$

where $g_2(E)$ is the Green's function of isolated contact 2: $(E - H_2)g_2 = I$.

As easily the Green's function for the device in the connected system, $G_d$, can be calculated. From the definition of Green's function and from equation 2.31

$$\begin{pmatrix} E - H_1 & -\tau_1 & 0 \\ -\tau_1^\dagger & E - H_d & -\tau_2^\dagger \\ 0 & -\tau_2 & E - H_2 \end{pmatrix} \begin{pmatrix} G_1 & G_{1d} & G_{12} \\ G_{d1} & G_d & G_{d2} \\ G_{21} & G_{2d} & G_2 \end{pmatrix} = \begin{pmatrix} I & 0 & 0 \\ 0 & I & 0 \\ 0 & 0 & I \end{pmatrix}, \tag{2.35}$$

which ultimately[2] gives

$$G_d = (E - H_d - \Sigma_1 - \Sigma_2)^{-1}, \tag{2.36}$$

where $\Sigma_1 = \tau_1^\dagger g_1 \tau_1$ and $\Sigma_2 = \tau_2^\dagger g_2 \tau_2$ are called self-energies and $g_{1,2}$ are the Green's functions of the isolated contacts. Self-energies describe the connection to electron sink or source and take into account the perturbative effect of the contacts. In

[2] See [48] for details.

general, matrix form of a Green's function in region $\alpha$ can be then evaluated by:

$$G_\alpha = (ES_\alpha - H_\alpha - \sum_i \Sigma_i)^{-1}, \tag{2.37}$$

where $\Sigma_i$ takes into account the effect of the neighboring region, $i$, and $S_\alpha$ is the overlap matrix.

When the Green's function of the device in the perturbed system is known, the total current flowing through the device can be defined by the Landauer formula for current:

$$I = \frac{e}{\pi\hbar}\int_{E=-\infty}^{\infty} dE(f(E,\mu_1) - f(E,\mu_2))\mathrm{Tr}(G_d^\dagger \Gamma_2 G_d \Gamma_1), \tag{2.38}$$

where $f(E,\mu_{1/2})$ is the Fermi function and

$$\Gamma_j = i(\Sigma_j - \Sigma_j^\dagger).[33] \tag{2.39}$$

## 2.3 Theory of STM

Theory of scanning tunneling microscope focuses on how to derive the tunneling current between the STM tip and STM surface. Over the years numerous theories for calculating the tunneling current have been developed [29]. The theories are divided to four main categories [28]: Tersoff-Hamann approach [31], Bardeen's approach [30], Landauer-Büttiker approach [32] and Keldysh (NEGF) approach [33]. Here the theory of scanning tunneling microscope is presented according to Todorov and Pendry [35, 36].

To calculate the electrical current between two regions, A and B, the regions are at first thought of as separate systems (see picture 2.7). While the regions are isolated from each other, they have separate eigenstates, $E_A$ and $E_B$, and eigenfunctions, $\varphi_A$ and $\varphi_B$. In $B$ region $\varphi_A = 0$, and in $A$ region $\varphi_B = 0$. The Schrödinger equation of each isolated region is:

$$E_I\varphi_I = H_I\varphi_I, \tag{2.40}$$

where the subscript $I$ denotes isolated region $A$ or $B$. (This is a notation used throughout the section.)

When the regions are brought close to each other, a connection arises and tunneling between the regions is possible. A potential difference $v_{AB}$ appears between the regions. The amount of electrons of region $A$ to tunnel to region $B$, $\delta\varphi_{BA}$, can be derived from the Lippmann-Schwinger equation 2.29. Moving of the electrons from region to another gives rise to a current between the regions.

$$\delta\varphi_{BA} = G^0_{BB}T_{BA}\varphi_A, \tag{2.41}$$

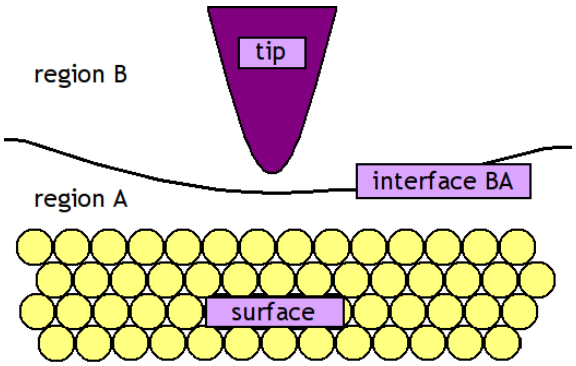


Figure 2.7: The $A$ and $B$ regions are in the STM model the tip and surface region. The tunneling current is calculated as the flowing current through interface $BA$.

where $G^0_{II}$ is the Green's function of an isolated region

$$G^0_{II} = \frac{1}{E - E_I - \Sigma_I} \tag{2.42}$$

and $T_{IJ}$ is transition matrix [45] that sums the series

$$T_{IJ} = v_{IJ}(1 - G^0_{II} v_{IJ} G^0_{JJ} v_{JI})^{-1}. \tag{2.43}$$

Here $v_{BA}$ is the scattering potential due to which electrons from $A$ travel to the $B$ region, and $T_{BA}$ is a modification of the potential $v_{BA}$ that takes into account multiple scattering. The $\Sigma_I$ term in 2.42 is the self-energy term as introduced in section 2.2.1.

$\delta\varphi_{BA}$ can be proven to obey the Schrödinger equation within $B$ region:

$$E\delta\varphi_{BA} = -\frac{\hbar^2}{2m}\nabla^2\delta\varphi_{BA} + V\delta\varphi_{BA} + \Sigma_B\delta\varphi_{BA}. \tag{2.44}$$

Now the equation 2.44 is multiplicated by $\delta\varphi^*_{BA}$ and a complex conjugate is taken of it. This gives:

$$E\delta\varphi_{BA}\delta\varphi^*_{BA} = -\frac{\hbar^2}{2m}\delta\varphi^*_{BA}\nabla^2\delta\varphi_{BA} + V\delta\varphi_{BA}\delta\varphi^*_{BA} - \delta\varphi_{BA}\Sigma^*_B\delta\varphi^*_{BA}. \tag{2.45}$$

and the complex conjugate:

$$E\delta\varphi^*_{BA}\delta\varphi_{BA} = -\frac{\hbar^2}{2m}\delta\varphi_{BA}\nabla^2\delta\varphi^*_{BA} + V\delta\varphi^*_{BA}\delta\varphi_{BA} + \delta\varphi^*_{BA}\Sigma_B\delta\varphi_{BA}. \tag{2.46}$$

Subtracting equation 2.46 from equation 2.45 and integrating over region $B$ leads to equation

$$2i\int_B \delta\varphi^*_{BA}\Gamma_B\delta\varphi_{BA}dB = \frac{\hbar^2}{2m}\int_B(\delta\varphi^*_{BA}\nabla^2\delta\varphi_{BA} - \delta\varphi_{BA}\nabla^2\delta\varphi^*_{BA})dB, \tag{2.47}$$

where

$$\Gamma_B = \frac{1}{2i}(\Sigma_B - \Sigma^*_B). \tag{2.48}$$

The right hand side of equation 2.47 can be transformed into a surface integral by using Green's theorem[3]:

$$2i\int_B \delta\varphi^*_{BA}\Gamma_B\delta\varphi_{BA}dB = \frac{\hbar^2}{2m}\oint_B(\delta\varphi^*_{BA}\nabla\delta\varphi_{BA} - \delta\varphi_{BA}\nabla\delta\varphi^*_{BA})d\vec{S}, \tag{2.49}$$

The integrand on the right hand side is clearly the formula of electrical current

$$I_{BA} = \frac{i\hbar e}{2m}(\delta\varphi^*_{BA}\nabla\delta\varphi_{BA} - \delta\varphi_{BA}\nabla\delta\varphi^*_{BA})[38]. \tag{2.50}$$

Combining this equation with equation 2.41 and 2.49, the current between the regions $A$ and $B$ is obtained:

$$I_{AB} = \frac{2e}{\hbar}\int_B \varphi^*_A T_{AB}G^{0-}_B\Gamma_B G^{0+}_B T_{BA}\varphi_A dB. \tag{2.51}$$

This corresponds the current formula given by Todorov:

$$dI_{AB} = \frac{2\pi e}{\hbar}\mathrm{Tr}[\rho^0_A T_{AB}\rho^0_B T_{BA}]dE, \tag{2.52}$$

where $\rho^0_{A/B}$ is unperturbed density of states as defined in equation 2.8 in the unperturbed scheme. As Pendry says though, this current only represents the contribution of a single 'mode'. This current is from the right lead and equal to the current from left lead as the voltage is zero. To receive the total current $I$, bias voltage $V$ is added. This changes the Fermi-Dirac distributions, that is the Fermi functions, in $A$ and $B$ regions to $f(E)$ and $f(E+eV)$, respectively.

The total current $I$ in the system is then obtained by multiplying the currents 2.52 of both regions by their distributions and subtracting them from each other:

$$\begin{aligned} I &= \int [dI_{AB}(E)f(E) - |dI_{BA}(E)|f(E+eV)] \\ &= \frac{2\pi e}{\hbar}\int \mathrm{Tr}[\rho^0_A(E)T^\dagger_{AB}(E)\rho^0_B(E)T_{BA}(E)][f(E) - f(E+eV)]dE. \end{aligned} \tag{2.53}$$

The Fermi functions are step functions as is seen in picture 2.8, so they pick up

[3]Green's theorem: $\int_V(u\nabla^2 v - v\nabla^2 u)d\alpha = \oint_{\partial V}(u\nabla v - v\nabla u)d\alpha$. [43]

the values up to energy $E_F$ ($f(E)$) and up to $E_F - eV$ in $f(E + eV)$. When these occupation functions are subtracted from each other, they form a function that picks up values in the range from $E_F - eV$ to $E_F$, which is the interesting energy region in this case.

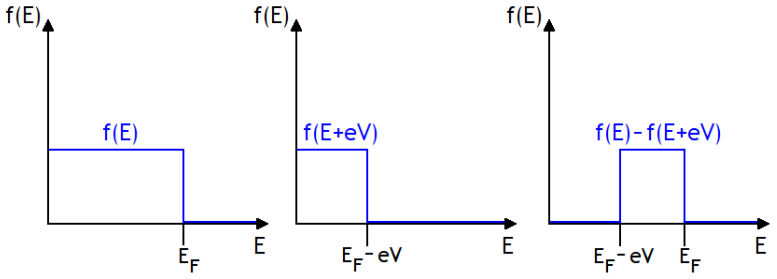


Figure 2.8: Fermi functions $f(E)$, $f(E + eV)$ and their remainder.

From the current formula, an equation for conductance, $\sigma$, is derived by simply differentiating the current with respect to voltage:

$$\sigma = \frac{dI}{dV} = \frac{2\pi e}{\hbar} \int [f(E) - f(E + eV)] \frac{d}{dV} \mathrm{Tr}[\rho_A^0(E) T_{AB}^\dagger(E) \rho_B^0(E) T_{BA}(E)] \\ + ef'(E + eV) \mathrm{Tr}[\rho_A^0(E) T_{AB}^\dagger(E) \rho_B^0(E) T_{BA}(E)] dE. \quad (2.54)$$

If the Fermi function is regarded as a step function as in picture 2.8, differentiating $f(E + eV)$ with respect to $V$ gives a negative delta-peak at $E + eV$. Hence the conductance takes a more convenient form

$$\sigma = \frac{dI}{dV} = \frac{2\pi e}{\hbar} \mathrm{Tr}[T_{AB} \rho_B^0(E_F) T_{BA} \rho_A^0(E_F + eV)][35], \quad (2.55)$$

if the density of states changes sufficiently slowly with respect to the bias voltage.

If this is compared to the Landauer formula of conductance [32]:

$$\sigma = \frac{e^2}{\pi\hbar} \mathcal{T}(E), \quad (2.56)$$

the transmission coefficient $\mathcal{T}(E)$ is received as

$$\mathcal{T}(E) = \frac{2\pi^2}{e} \mathrm{Tr}[T_{AB} \rho_\beta^0(E_F) T_{BA} \rho_A^0(E_F + eV)], \quad (2.57)$$

which is equal to the equilibrium limit of the non equilibrium equation

$$\mathcal{T}(E) = \frac{1}{e} \mathrm{Tr}[G_d^\dagger \Gamma_2 G_d \Gamma_1]. \quad (2.58)$$

Another thing to be noted is the connection of equation 2.53 to Bardeen's tun-

neling current in equation 2.2. This implies that

$$I = \frac{2\pi e}{\hbar} \int \mathrm{Tr}[\rho_A^0(E)|M_{AB}|^2 \rho_B^0(E)][f(E) - f(E+eV)]dE, \tag{2.59}$$

which now corresponds to the finding of Tersoff and Hamann of the proportionality of current to local density of states (equation 2.5), as the basis is changed from $(A, B)$ to $(\mathbf{r}, \mathbf{r}')$.

Tersoff and Hamann's definition of the surface's wave function is

$$\psi_A(\mathbf{r}_0) \propto e^{-2\kappa(R+d)}, \tag{2.60}$$

where $R$ is the radius of curvature of the tip and $d$ is smallest distance between tip and surface. This means that the tunneling current must be proportional to the distance between tip and surface

$$I \propto e^{-2\kappa d}. \tag{2.61}$$

This is the exact same as presented in equation 2.1. This also leads to a conclusion that the conductance has also a similar dependency on the distance $d$:

$$\sigma \propto e^{-2\kappa d}.[31] \tag{2.62}$$

# 3. SIMULATION METHODS

To simulate realistic STM experiments, detailed information about the system's geometric and electronic structure is essential. In simulations the aim is to create a system that is geometrically as close to a real system as possible, and to have as accurate electronic structure of it as possible. Reaching the optimal geometric structure and the corresponding electronic structure of the many-body system involves solving its Schrödinger equation. To solve the Schrödinger equation of a complex many-body system, approximations to the equation have to be made, which are introduced by electronic structure methods.

Density functional theory, DFT, [49, 50] has become a popular electronic structure method for studying materials and molecules at the atomic scale [51]. In DFT the ground state energy of an electronic system is written in terms of electron probability density, $\rho(\mathbf{r})$, which denotes the total electron density at a particular point $\mathbf{r}$ in space. The energy is thus a functional of the electron density, $E[\rho(\mathbf{r})]$. This method enables an accurate and efficient way of solving systems with hundreds of atoms. For calculations of the excited energy states a time-dependent density functional theory, TDDFT is used. [52]

In this thesis, all the simulations are done using a grid-based projector augmented wave (GPAW) method. GPAW is an open source density functional theory Python [53] code that implements projector augmented-wave method, PAW, [54] using a real space grid [51]. Instead of using a grid, GPAW can also perform the calculation by using a localized atomic-orbital basis set. With the localized atomic-orbital basis set GPAW can be used for studying of scanning tunneling microscopy and electron transport using non equilibrium Green's functions. Non equilibrium Green's function method enables taking both the tip and surface structures into account in the simulation. The STM and transport simulations are thus a combination of DFT and NEGF method, which at present is actually the most popular approach to simulations of transport in nanocontacts [55]. Therefore, GPAW is the only simulation tool needed, and it seems to be a suitable choice for the calculations.

In this chapter the simulation methods of this thesis are presented. At first the used program package GPAW, and the PAW method it is based on, are introduced. The simulation methods used in electronic structure, STM and electron transport calculations follow. Curious readers can find all the used scripts in appendix A.

## 3.1 Grid-based projector augmented wave method

Grid-based projector augmented wave method, GPAW, [51] is the main method used in the calculations of this thesis. GPAW is a density functional theory (DFT) code that implements the projector augmented wave, PAW, [54] method using a real space grid. The use of a real space grid introduces several advantages: free and periodic boundary conditions can be flexibly treated, parallelization is efficient with small communication between computational cores, and accuracy is adjusted systematically by changing the grid spacing. When no such accuracy is needed, GPAW uses atom-centered localized orbitals. This is called the LCAO mode, the LCAO denoting linear combination of atomic orbitals. LCAO mode is used for example in electron transport calculations within non equilibrium Green's function approach. [56] The grid presentation and LCAO mode can be combined to receive optimal performance. For example a structural optimization can be performed by first optimizing within LCAO mode and then changing to grid mode to receive for example adsorption energies, which would not be good in LCAO. [57]

In the following subsections an introduction to projector augmented wave method is provided and characteristics of grid and LCAO mode are presented. For a more detailed information about PAW method and GPAW and its parameters, the references [56, 54, 58, 51] are recommended.

### 3.1.1 Projector augmented wave method

Projector augmented wave method, PAW, was introduced by Blöchl in 1994 [54]. This ab initio electronic structure method combines the augmented wave methods [59] and the pseudopotential approach [60]. As input the method requires only the charge and mass of the nuclei, the number of electrons and an initial atomic geometry [61]. The theory introduced here follows the paper of Rostgaard [58].

In PAW method the original rapidly oscillating Kohn-Sham single particle wave functions $|\psi_n\rangle$ near the nuclei are written with the help of auxiliary smooth pseudo wave functions $|\tilde{\psi}_n\rangle$:

$$|\psi_n\rangle = \hat{T}\,|\tilde{\psi}_n\rangle\,, \tag{3.1}$$

where $n$ labels the quantum state and $\hat{T}$ is linear transformation operator. The auxiliary wave functions can then be solved from transformed Kohn-Sham equations[1]:

$$\hat{T}^\dagger \hat{H} \hat{T}\,|\tilde{\psi}_n\rangle = \epsilon_n \hat{T}^\dagger \hat{T}\,|\tilde{\psi}_n\rangle\,, \tag{3.2}$$

where $\epsilon_n$ is the energy of the corresponding single particle wave function $|\psi_n\rangle$.

It is notable that the transformation has effect only inside a certain atom-specific

[1] Kohn-Sham equation is the Schrödinger equation of a system of non-interacting particles. [50]

augmentation region, called augmentation sphere, for which

$$|\bar{r} - \bar{R}^a| < r_c^a, \tag{3.3}$$

where $\bar{r}$ is the position vector, $\bar{R}^a$ is atom $a$'s position and $r_c$ is the cutoff radius of the augmentation sphere of atom $a$. The augmentation spheres do not overlap. Inside the augmentation sphere the real wave function is expanded into partial waves $\phi_i^a$, which each have their own corresponding auxiliary smooth partial wave $\tilde{\phi}_i^a$. Outside the augmentation sphere the transformation must not have an effect, because the wave functions are already smooth there. The transformation is defined

$$\hat{T} = 1 + \sum_a \sum_i \hat{T}^a \left|\tilde{\phi}_i^a\right\rangle \left\langle \tilde{p}_i^a\right| = 1 + \sum_a \sum_i (|\phi_i^a\rangle - |\tilde{\phi}_i^a\rangle) \left\langle \tilde{p}_i^a\right| . \tag{3.4}$$

The transformation is expressed in terms of partial waves, smooth partial waves and smooth projector functions, $\tilde{p}_i^a$. The projector functions are localized inside the augmentation spheres and satisfy $\langle \tilde{p}_{i_1}^a | \tilde{\phi}_{i_2}^a \rangle = \delta_{i_1 i_2}$.

For calculating densities and energies, PAW method uses the same approach. Inside the augmentation sphere the parameter under examination is smooth, and as $r > r_c^a$ it meets the unsmooth value. Because going through all the details of PAW is not of importance here, the references [54, 51] are recommended. The electron densities and total energies as well as the construction of projector functions and smooth waves in PAW are described there.

In the calculations performed, the Hamiltonian and overlap matrices are often received straight from GPAW calculator. In projector augmented wave method the Hamiltonian is:

$$\tilde{H} = -\frac{1}{2}\nabla^2 + \tilde{v} + \sum_{aij} \left|\tilde{p}_i^a\right\rangle \Delta H_{ij}^a \left\langle \tilde{p}_j^a\right| , \tag{3.5}$$

where $\tilde{v}$ is the effective potential, $|\tilde{p}_i^a\rangle$ are localized functions that are nonzero inside an augmentation sphere around each atom $a$, and $\Delta H_{ij}^a$ atomic Hamiltonians that contain the local contribution of individual atoms. The Hamiltonian for any two basis functions, with overlap with the augmentation spheres ignored, is:

$$H_{ij} = \langle \Phi_i | \tilde{H} | \Phi_j \rangle \approx \langle \Phi_i | - \frac{1}{2}\nabla^2 + \tilde{v} | \Phi_j \rangle . \tag{3.6}$$

The overlap between two basis functions is defined through an overlap operator

$$S = 1 + \sum_{aij} \left|\tilde{p}_i^a\right\rangle \Delta S_{ij}^a \left\langle \tilde{p}_j^a\right| , \tag{3.7}$$

where $\Delta S_{ij}^a$ are the atomic contributions defined by

$$\Delta S_{ij}^a = \langle \phi_i^a | \phi_j^a \rangle - \langle \tilde{\phi}_i^a | \tilde{\phi}_j^a \rangle \,. \tag{3.8}$$

The overlap is

$$S_{ij} = \langle \phi_i | \phi_j \rangle + \sum_{aij} \langle \phi_i | \tilde{p}_i^a \rangle \, \Delta S_{ij}^a \, \langle \tilde{p}_j^a | \phi_j \rangle \,. \tag{3.9}$$

If the centers of the basis functions are far apart, the atomic contributions can be ignored and the overlap matrix approximated by:

$$S_{ij} \approx \langle \phi_i | \phi_j \rangle \,. \tag{3.10}$$

### 3.1.2 Grid mode

In GPAW's grid mode wave functions, electron densities and potentials are represented on tridimensional uniform grids in real space. All integrals over space are turned into sums over the grid points. The grid is defined by its spacing $h$, which defines the accuracy of the calculation: the smaller the grid spacing the more accurate the calculation. The grid is illustrated in two dimensions in figure 3.1. For calculation of the wave functions a coarse grid is used, and for electron densities and potentials a fine grid. The fine grid has twice as many grid points as the coarse grid in each direction and its grid point density therefore is $2^3 = 8$ times higher. [51]

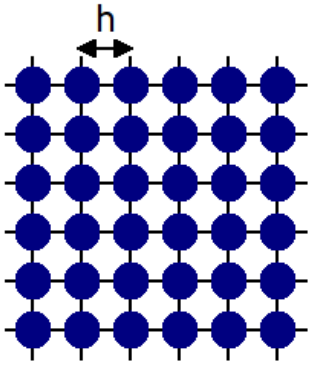


Figure 3.1: In GPAW's grid mode the system is defined on a uniform real space grid with grid spacing $h$.

Boundary conditions can be defined in the grid as zero for isolated systems and periodic for periodic systems. In the calculations of this thesis, **k**-point sampling is used, and therefore wave functions have Bloch type boundary conditions

$$\tilde{\psi}_{n\mathbf{k}}(\mathbf{r} + \mathbf{R}) = \tilde{\psi}_{n\mathbf{k}}(\mathbf{r}) e^{i\mathbf{k}\cdot\mathbf{R}}, \tag{3.11}$$

where $\mathbf{R}$ is any Bravais vector. [56]

### 3.1.3 LCAO mode

LCAO mode is not as numerically accurate as the grid mode, but it offers a computationally effortless and more efficient way of computing in GPAW. LCAO mode and grid mode can be used side by side, starting for example with LCAO mode and completing the results with grid mode to receive more accurate results.

In LCAO mode the wave functions are written as a linear combination of atomic-like orbitals $\Phi_v(\mathbf{r})$

$$\tilde{\Psi}_n(\mathbf{r}) = \sum_v c_{nv}\Phi_v(\mathbf{r}), \tag{3.12}$$

where $c_{nv}$ are the expansion coefficients. The atomic-like orbitals used as basis functions $\Phi_v(\mathbf{r})$ are atom centered and of the form:

$$\Phi_v(\mathbf{r}) = \Phi^a_{\ell mn}(\mathbf{r}) = R^a_{n\ell}(|\mathbf{r} - \mathbf{R}^a|)Y_{\ell m}(\mathbf{r} - \mathbf{R}^a), \tag{3.13}$$

as $v$ is a composite of $a$, $n$, $\ell$ and $m$ (the principal, angular momentum and magnetic quantum numbers), $R^a_{n\ell}$ is the radial function and $Y_{\ell m}$ is the spherical harmonic. The basis function is strictly localized and thus vanishes beoynd a certain cutoff radius $r_c$. [56] This sets the Hamiltonian and overlap matrices sparse in the basis-set representation [57].

The accuracy received using the LCAO mode depends on the quality of the basis set that is chosen to represent the electronic structure. The simplest basis set is the single zeta basis, sz, which contains one atomic orbital per valence electron. To improve radial flexibility, basis functions with the same angular momentum $\ell$ can be added to each valence state. The basis is then called a multiple-zeta basis, which can be denoted as dz or tz as the basis is double-zeta or triple-zeta. For improvement of the angular flexibility, polarization functions are added. In these functions $\ell$ corresponds to the lowest unoccupied angular momentum. With the polarization functions added the basis are called single-zeta polarized, szp, double-zeta polarized, dzp and so on. [56] The used basis defines the number of basis functions, which is an essential piece of information in some parts of the STM and transport calculations.

In STM and transport calculations the spatial resolution is essential, so the physically intuitive local real space basis of LCAO is very useful. Another redeeming feature is the lower computational cost, which is significant in examination of large systems. Hence, in the STM and transport calculations of this thesis, the LCAO mode is applied.

## 3.2 Calculation of the electronic structures

Knowledge of the geometric and electronic structure is essential in STM calculations. To build atomic structures, Atomic Simulation Environment, ASE, [62] is used. ASE works in cooperation with a calculator, in this thesis mainly GPAW[2], which provides for example the energies, forces and wave functions. Then in optimizing structures, the calculator solves new positions for the atoms using the defined quality.

The structure optimizing works as follows. At first a starting geometric structure must be defined with ASE. Then a calculator is added to define properties, such as the electronic structure, of the defined geometric structure. The electronic structure is needed to define forces between atoms. The interest is in finding out what is the optimal geometrical structure of the given system. Thus, the optimization calculation runs until the force, $\vec{F}$, on all individual atoms, $a$, is less than the maximum force $f_{\max}$ defined:

$$\max_a |\vec{F}_a| < f_{\max}. \tag{3.14}$$

Eventually as a result is given an optimal geometrical structure and the corresponding electronic structure, just what is needed for STM calculations.

## 3.3 STM calculations

GPAW includes an STM code for calculating STM images and corrugation curves using non equilibrium Green's functions. It has been used in previous STM calculations [65, 66], but later on its functionality has been questioned [67]. Method uses Bardeen's theory [30] to calculate the tunneling current. Bardeen's approach keeps the wave functions of tip and surface separate and fixed, and thus does not offer a realistic model to STM calculations, when the tip and surface are brought very close or a large bias voltage is applied, which would cause distortion to the wave functions. The method is limited to large tip to surface distances and low bias voltage, but within these limitations it is a succesfull and widely used method. [65]

As seen in subsection 2.2.1 the standard NEGF treatment divides the system into three subsystems. However, in the STM code used in this thesis the tip and suface are represented as two separate subsystems as in Bardeen's approach. This is due to the fact that in STM calculations it is vital that the tip is allowed to move arbitrarily with respect to the surface plane. The subsystems are in thermal equilibrium and coupling between them is treated perturbatively. They consist of a non-periodic part and a semi-infinite bulk crystal which are coupled. The STM system is illustrated in figure 3.2.

The Hamiltonian of the whole STM system, $H$, can then be constructed of the

[2]Effective medium theory (EMT) potential [63, 64] is the other one used in the calculations.

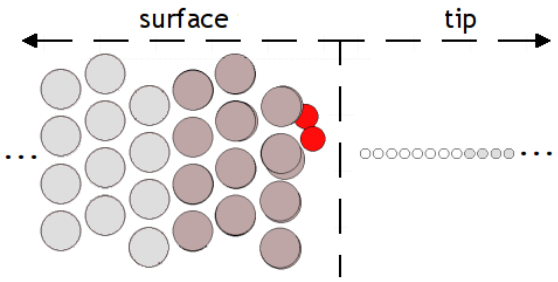


Figure 3.2: Model picture of the STM system, which is divided to tip and surface regions. The light grey atoms illustrate the semi-infinite part of the regions.

Hamiltonians of isolated tip and region, $H_S$ and $H_T$, and the coupling in between, $V$:

$$H = H_S + H_T + V. \tag{3.15}$$

The elements of the coupling matrix are calculated from overlaps of particular basis functions in the tip and surface region, $|\phi_t\rangle$, $|\psi_s\rangle$:

$$V_{TS} = \langle\phi_t|H_{TS}|\psi_s\rangle = \langle\phi_t| - \frac{1}{2}\nabla^2 + V_{KS}^T + V_{KS}^S|\psi_s\rangle\,, \tag{3.16}$$

where $V_{KS}^\alpha$ is the Kohn-Sham potential [50] of an isolated region $\alpha$.

The tunneling current, as the applied bias voltage is $U$, is calculated as

$$I = \frac{2e^2}{h}\int_{E_F}^{E_F+eU} dE \mathrm{Tr}\big[V_{ST}A_{TT}(E-eU)V_{TS}A_{SS}(E)\big], \tag{3.17}$$

where the integration is over the bias window $eU$ and

$$A_{\alpha\alpha} = i\big[G_{\alpha\alpha}^- - G_{\alpha\alpha}^+\big]. \tag{3.18}$$

$A_{\alpha\alpha}$ is the spectral function for isolated region $\alpha$, where $G^+$ and $G^-$ are the retarded and advanced Green's functions

$$G_{\alpha\alpha}^+(E) = [(E+i\eta)S_\alpha - H_\alpha - \Sigma_\alpha]^{-1} \tag{3.19}$$

$$G_{\alpha\alpha}^-(E) = [(E-i\eta)S_\alpha - H_\alpha - \Sigma_\alpha]^{-1}. \tag{3.20}$$

Equation 3.17 is equal to the Bardeen's formula of current presented in equation 2.53. The connection of the formulas is discussed in detail in reference [66].

To receive the Hamiltonians and overlap matrices for tip and surface, DFT calculations must be done and the structure must be optimized. Because the regions are divided to a periodic and non periodic part, the calculations are done to each part separately. Division to semi-infinite and non-periodic parts is illustrated nicely

in picture 3.4, which demonstrates the almost identical transport calculation setup.

In calculations the periodic semi-infinite part is constructed of infinitely repeated principal layers. These principal layers must be thick enough to ensure that coupling takes place only between neighboring layers. The principal layers must also be compatible with the structure at issue. If a surface has an fcc(111)[3] structure, the principal layers posited side by side must construct an fcc(111) structure. Thus the number of atomic layers constructing the principal layers depends on the crystal structure: fcc(111) needs three atomic layers and fcc(100) settles with two (see picture 3.3). Calculation of the Hamiltonian and overlap matrices for one principal layer is sufficient to receive the useful information for the semi-infinite part.

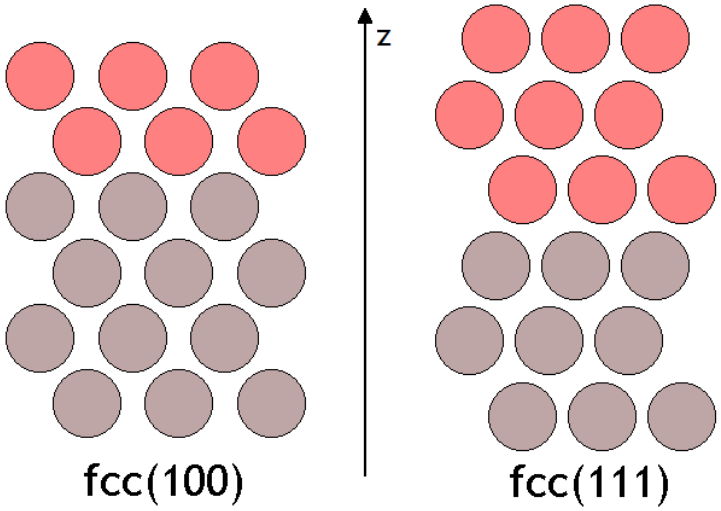


Figure 3.3: Fcc(100) and fcc(111) structures in the xz-view. Red atoms show the structure that is replied in the z-direction.

The non-periodic part is only periodic in the transverse direction, and thus surrounded by a vacuum on both sides in the transport direction. For a smooth matching in the interface of the non-periodic and semi-infinite part, a couple of convergence layers are to be added on the other side of the non periodic part. The convergence layers take care that the potential in the non-periodic part converges to the bulk value present in the semi-infinite lead. The convergence layers are removed after the DFT calculation is performed.

After the structure has been optimized and the DFT calculation is done, Green's functions are defined by equation 2.37, coupling between tip and surface for all tip positions by equation 3.16, and at last the tunneling current as presented in equation 3.17.

The code calculates constant height STM images. Constant current STM is done

[3]fcc = face centered cubic

by mapping the current as a function of positions $x$, $y$ and tip height $d$. Then to receive constant current image for a particular current, the corresponding image is found by interpolating between constant height images.

## 3.4 Transport calculations

Transport calculations are done following the example scripts in GPAW's homepages. Script uses ASE's TransportCalculator class to calculate the transmission functions and GPAW calculator to receive the Hamiltonians and overlap matrices. TransportCalculator applies the Green's function method to define transport properties of a device trapped between two semi-infinite leads. The class also introduces the calculation of projected density of states.

In transport calculations the system is divided to a central region and two semi-infinite leads on both sides of the central regions [56]. The semi-infinite leads are constructed of infinitely repeated principal layers, as was done in the STM calculations. The central region contains at least one principal layer on each side and the region must be large enough to ensure there is no direct coupling between the leads. The principal layer size is defined to be large enough to ensure coupling only takes place between nearest neighbor layers. A model of division into the central and lead regions is presented in picture 3.4.

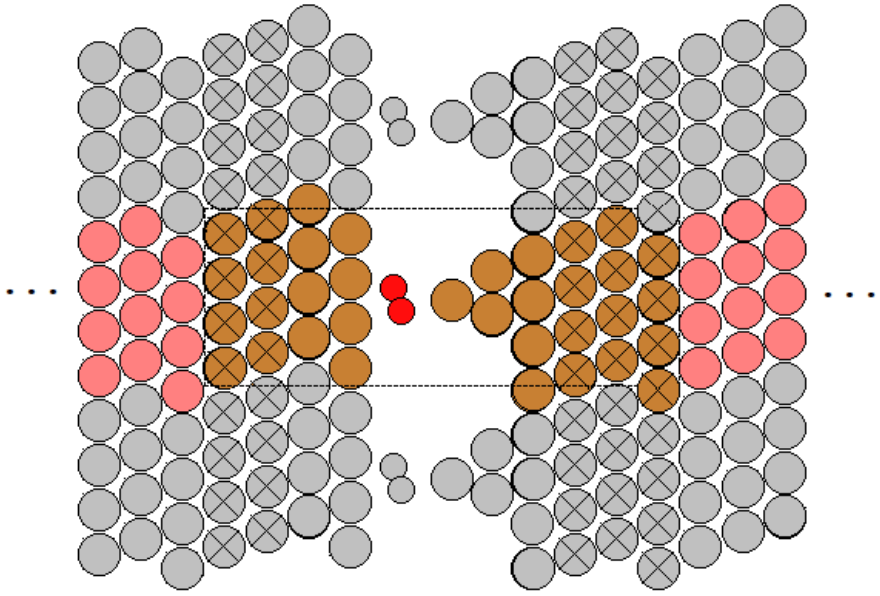

Figure 3.4: In ASE's transport module the system is constructed of a central region (the brown and red atoms in the middle in the box) and of principal layers (pink atoms) that are repeated infinitely. The principal layers construct the semi-infinite leads. The three layers of pink atoms represent one principal layer. Grey atoms demonstrate the periodicity in the transverse direction.

The system is described by a Hamiltonian whose each term is ascribed as left,

central or right region or the coupling between the regions. The Hamiltonian is hence written as a block tridiagonal matrix:

$$H = \begin{pmatrix} \ddots & V_L & & & \\ V_L^\dagger & H_L & V_L & & \\ & V_L^\dagger & H_C & V_R & \\ & & V_R^\dagger & H_R & V_R \\ & & & V_R^\dagger & \ddots \end{pmatrix}, \tag{3.21}$$

where the Hamiltonians $H_{L/R}$ are for the left/right principal layer, $H_C$ for the central region and $V_{L/R}$ describes the coupling between principal layers and coupling from principal layers into the central region. $V_{L/R}$ corresponds to the $\tau_i$ defined in subsection 2.2.1.

The matrices $H_{L/R}$, $V_{L/R}$ and $H_C$ can be model Hamiltonians or received from different kinds of electronic structure codes. With $H_{L/R}$, $V_{L/R}$ and $H_C$ defined, the elastic transimission function is determined using the non equilibrium Green function (NEGF) method.

The method is simple, really. Once the Hamiltonians and overlap matrices, that is the coupling matrices, for the subsystems are constructed in LCAO basis, getting Green's functions and self-energies is straightforward: $H_L \rightarrow G_L$, $H_R \rightarrow G_R$ and $H_C \rightarrow G_C$, and the self-energies:

$$\Sigma_{L/R} = V_{L/R}^\dagger G_{L/R} V_{L/R}. \tag{3.22}$$

The transmission is finally received from equation 2.58, where $\Gamma_1 = \Gamma_L$ and $\Gamma_2 = \Gamma_R$, and they are defined according to equation 2.39. Projected density of states is calculated from Green's functions with formula 2.8.

# 4. SYSTEMS, SIMULATIONS, RESULTS AND ANALYSIS

The goal is to model scanning tunneling microscopy and electron transport. This is done using the calculation methods presented in chapter 3. All the calculations begin with defining and optimizing a geometric structure. The optimization gives the electronic structure: wave functions and energy levels are obtained. With electronic structure received the density of states and Green's functions can be calculated. Using the non equilibrium Green's function methods then allows the calculation of STM images and the transmission coefficient. The flowchart in figure 4.1 presents the calculation progress.

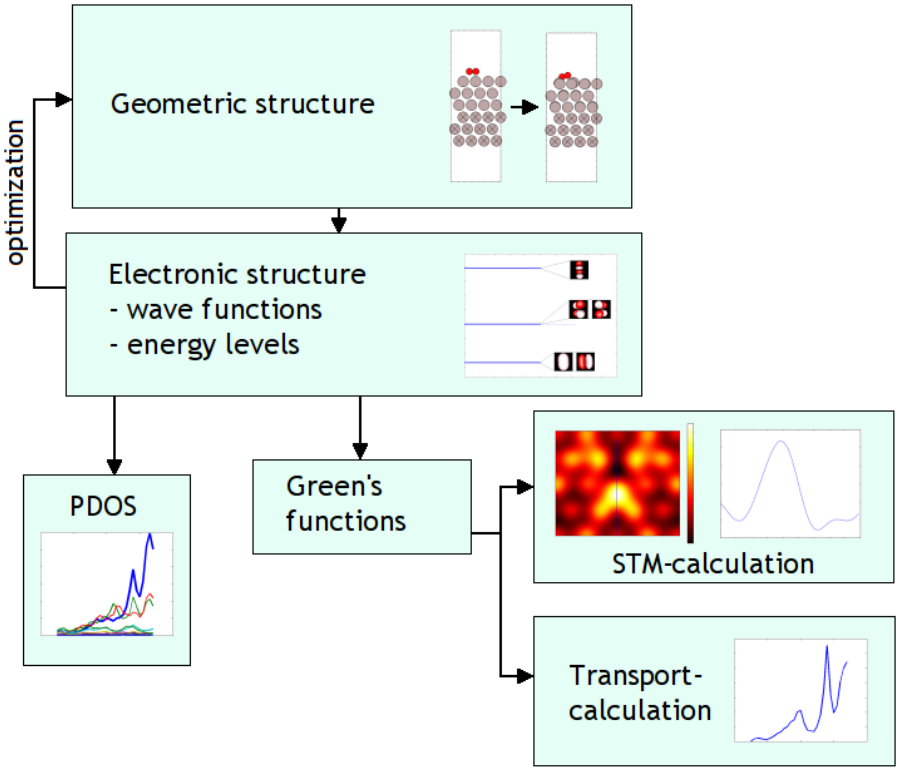


Figure 4.1: Flowchart of the calculations done.

In this chapter the systems and results of the simulations are presented. The structures examined are Cu(111) and Al(111) surfaces with and without $O_2$ and $H_2$

adsorbates. STM images for Cu(100) are also calculated. In addition to transport calculations the projected density of states are imaged to receive information of the transmission channels.

## 4.1 Electronic structure of $H_2$ and $O_2$

$H_2$ and $O_2$ are the adsorbates in the studied systems, so the electronic structures of the molecules are calculated. For the initial geometric structure experimental bond lengths [68] are applied. GPAW calculates the electronic structure automatically when a structure is optimized, giving the Fermi level, band eigenvalues and band occupancy. The wave function of each energy level is saved to plt-format, which can be opened in gOpenMol [69] to draw contour plots of each wave function.

The calculated electronic structures near the Fermi level can be seen in picture 4.2. Contour plots of the wave functions are attached to the energy level diagrams viewing the molecular orbitals of the corresponding energies. The figure shows a clear difference between the electronic structures of $H_2$ and $O_2$. For $H_2$ there are no energy levels near the Fermi level, as for $O_2$ the highest occupied molecular orbital, HOMO, and lowest unoccupied molecular orbital, LUMO, are degenerate and sited on the Fermi energy.

It should be noted that these molecules are isolated and as they are added to metal surfaces their energy states will shift and broaden, as is seen later. Because of the great difference in these molecules' electronic structures, they are expected to have a differing effect on the STM images and transport properties. This is why these two molecules in particular were chosen.

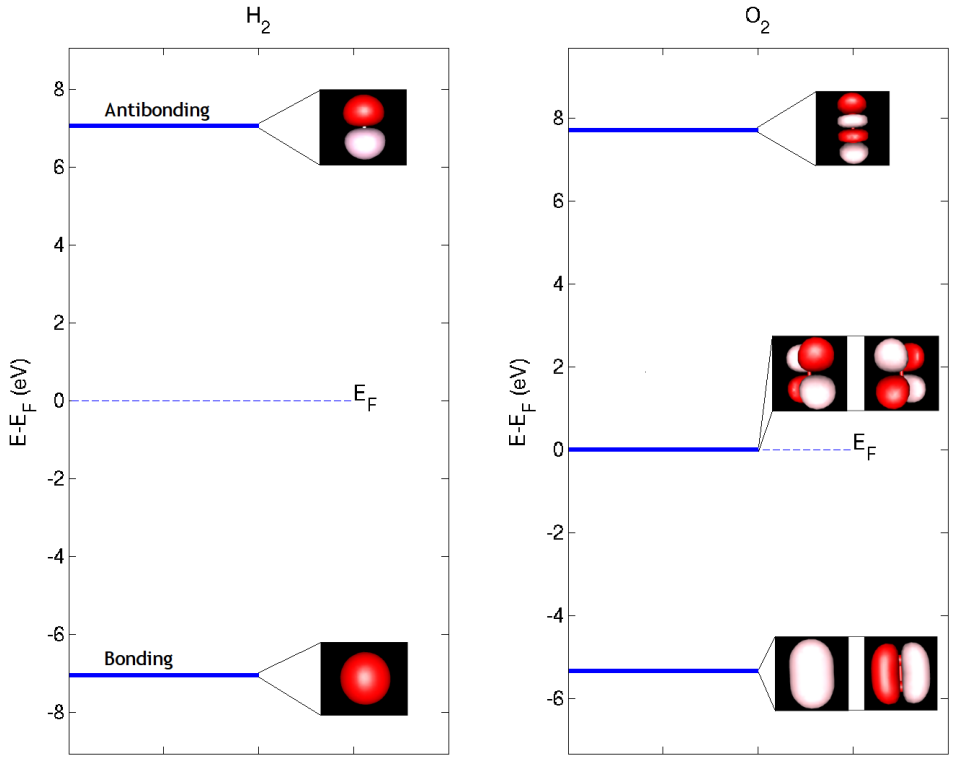


Figure 4.2: Energy levels and the corresponding wavefunctions of $H_2$ and $O_2$ near the Fermi level $E_F$.

## 4.2 STM images

STM images are calculated for Al(111), Cu(111) and Cu(100) surfaces. The exemplary GPAW's scripts are for Al(100) $2 \times 2 \times 9$ surface, so at first Cu(100) surface is studied. In the example script the tip consists of a long chain of hydrogen atoms. This is also the tip used in the STM calculations of this thesis. To ensure reliable results, the structures simulated are as large as possible and periodic boundary conditions are added in the plane of the surface.

The simulations are started with simulating small surfaces, first a $2\times2\times9$ Cu(100) surface. The bias voltage used is V = 0.05 eV and the number of both convergence and principal layers is 4. STM images are presented in figure 4.3. Images show a clear contrast change as the distance is increased from 4 Å to 5 Å. Unfortunately no constant current STM images are obtained.

For calculations of $2 \times 2 \times 9$ Cu(111) structure the same bias voltage is used, but the number of principal and convergence layers is decreased from four to three to take into account the change from fcc(100) to fcc(111) structure. Results are received, but the images are stretched. The obtained STM images should be of the

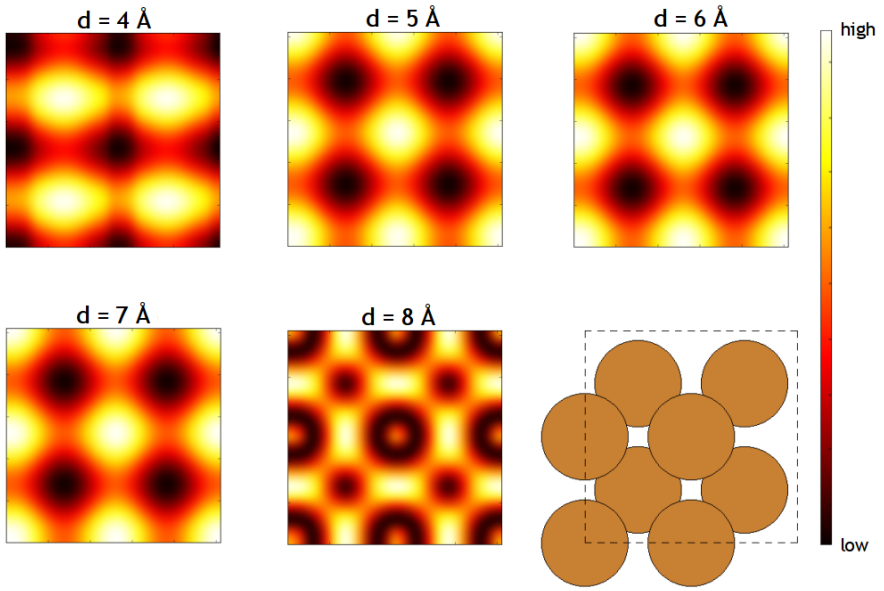


Figure 4.3: STM image for $2 \times 2 \times 9$ Cu(100) surface and structure's plane view.

same size and shape with the cell of the structure, but in these calculations the resulting image stretches the x-coordinate to the length of y-coordinate of the cell and y to the length of x respectively. To receive sensible images, the images are scaled to the shape of the cell. The rescaled STM images of Cu(111) are in picture 4.4.

The constant height picture is calculated with 5 Å height and the height in constant current picture is ranging in around 6 Å, so the pictures are assumed to resemble each other. The pictures in figure 4.4 are not alike, though. The constant height picture seems to correspond the structure quite nicely, but the constant current picture has a strange wavy look. This implies that the unit cell size is too small and instead calculations for larger structures should be carried out. The problem arises from the periodicity of the small cell. If the cell is too small, the tip may see an atom and its image in the neighboring cell simultaneously, which distorts the results.

Unfortunately, STM simulations of larger copper surfaces are not successful. When trying to initialize the STM system, an error message is received, which claims that the atoms are too close to cell boundaries. It is suggested [70] that the error message means that the augmentation sphere is too large to fit in the cell. This means that the cutoff radius $r_c$ is slightly larger than the distance to the cell boundary. Browsing the GPAW mailinglist's messages further, it is found out that the STM code has a bug in it. The problem is that it depends on the system, whether the augmentation spheres are included in their entirety to the calculations. If they are not, the cutoff error arises. [71]

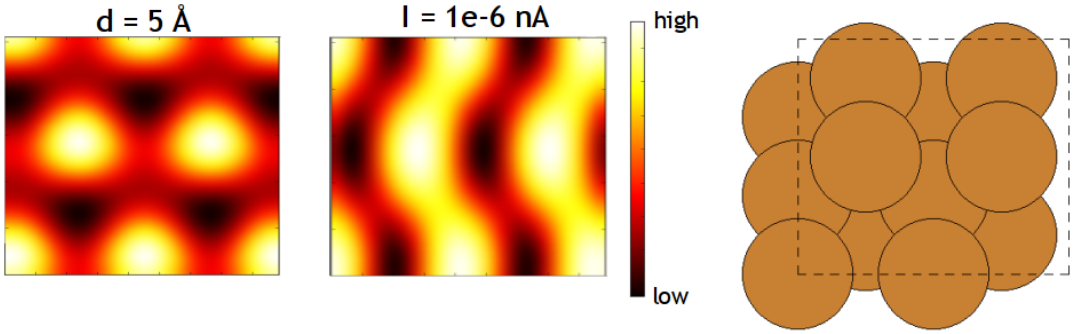


Figure 4.4: Calculated constant height and constant current STM images of small $2 \times 2 \times 9$ Cu(111) surface and the structure's xy-view.

Because the simulation of larger copper surfaces is not possible, an Al(111) surface is studied. Simulations for a clean $4 \times 4 \times 6$ Al(111) surface and for the same surface with $O_2$ adsorbate are carried out. The results can be seen in pictures 4.5, 4.6, 4.7 and 4.8. Pictures present constant height and constant current images calculated with various heights and currents. Before the actual STM simulation the structures are optimized. In the optimization the three bottom layers of the surface are kept in place and the three top layers are allowed to move. The bond length of $O_2$ is also constrained to remain constant. The optimized structures are presented with the STM images mentioned above.

The constant height and constant current images of the clean Al(111) surface are similar and correspond each other well. The constant current image with current $I = 1 * 10^{-3}$ nA with the tip height ranging between 7.35 Å and 7.40 Å looks about the same as the constant height image received with tip height of 7.5 Å. Most of the received images also seem to have $C_6$ rotational symmetry: the images can be rotated 60° and the image remains the same. This is correct, because the fcc(111) plane has the same $C_6$ symmetry.

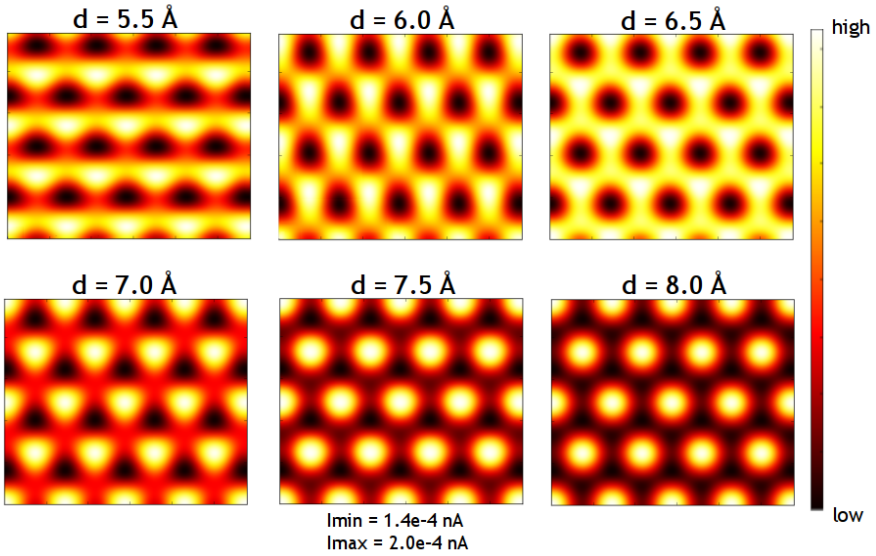


Figure 4.5: Constant height images of Al(111) surface at different heights, $d$. The magnitude of the current is simply illustrated by a light colour at the highest current and dark colour at the lowest current. The corresponding currents decrease as the tip is moved further, so same colours in different pictures do not represent same currents.

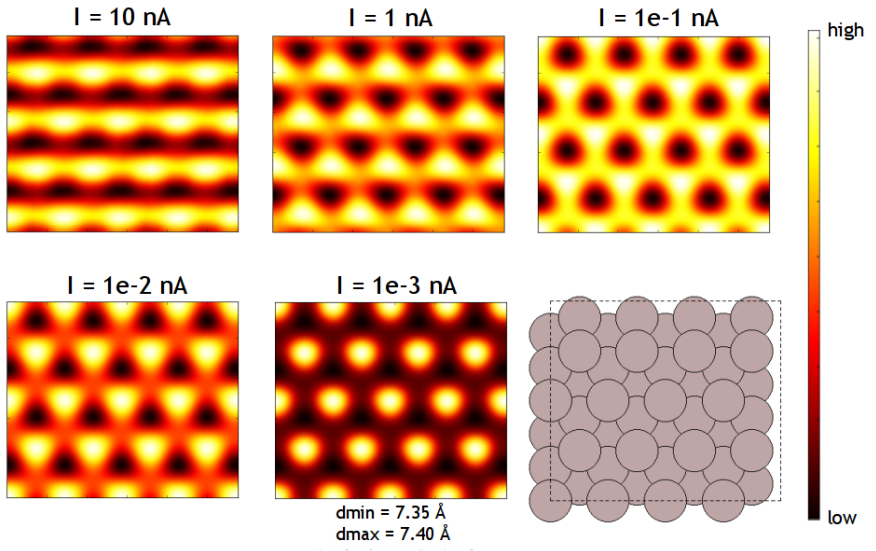


Figure 4.6: Constant current images of Al(111) surface at different currents. The lighter the colour, the further the tip is from the surface.

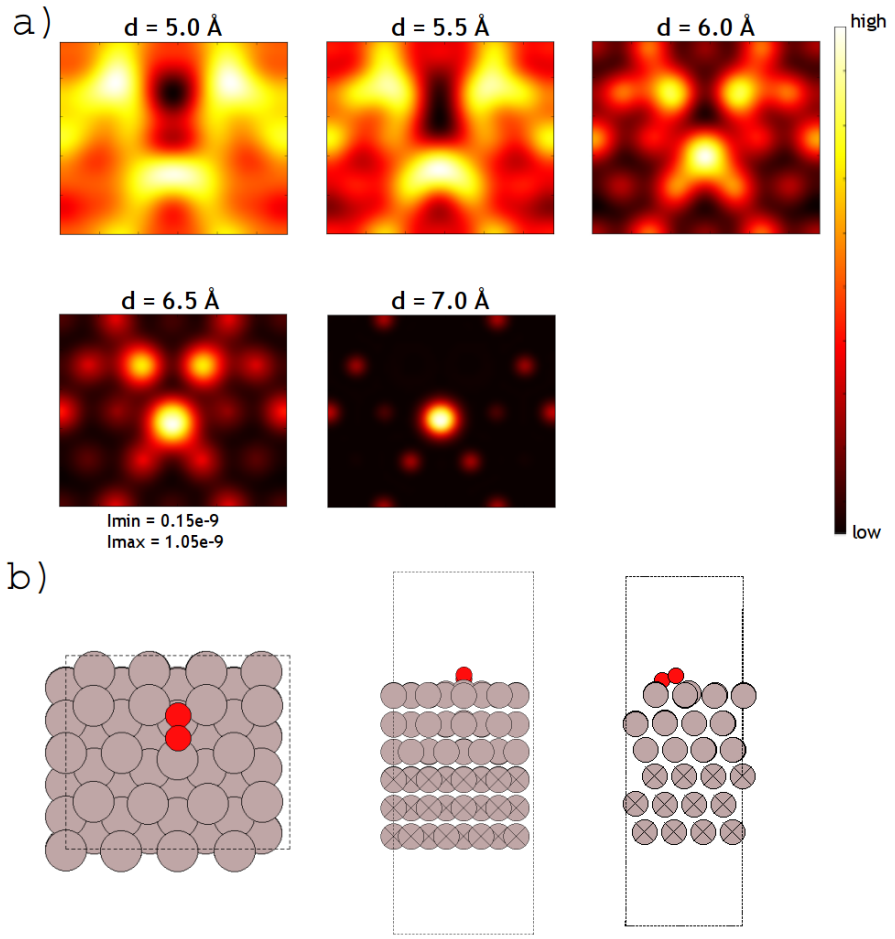


Figure 4.7: a) Constant height images of Al(111) surfaces with an $O_2$ adsorbate molecule. b) The xy-, xz- and yz-views of the optimized structure. The atoms with 'X' are set still in structure optimization.

STM images and the optimized structure of $O_2$ adsorbate on Al(111) surface is shown in figure 4.7. The optimized structure shows that the molecule is clearly higher than the aluminium surface and that it attracts the atoms of the aluminium surface from the plane. The higher oxygen atom of $O_2$ molecule is about 1.7 Å from the surface plane and the lower 1.3 Å. Three of the molecule's closest aluminium atoms have rised the most from the surface plane. Their distances from the surface plane are 0.2 Å, for the aluminium atom beneath the higher oxygen atom, and 0.1 Å, for the two other atoms.

Although the $O_2$ adsorbate is clearly higher than the aluminium surface plane, it is not observed in the STM images. Instead a depression is seen in the post of the adsorbate. Same kind of depressions are found in experimental results [72, 73]. The aluminium atoms that are higher than the surface plane are seen as protrusions, as would be expected. The $O_2$'s effect on the surface seems to be very wide. It is not

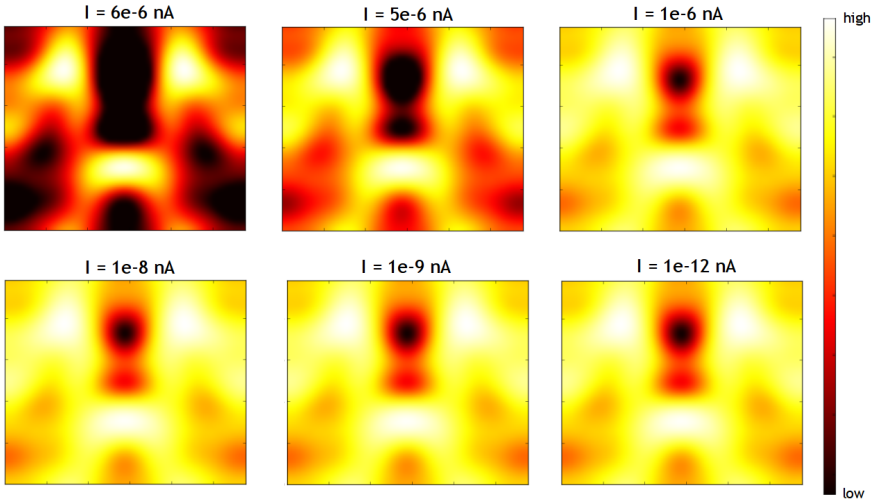


Figure 4.8: Constant current images of Al(111) surfaces with an $O_2$ adsorbate molecule. Strangely the distance between the tip and surface does not seem to change according to these images.

localized on the adsorption site, but seems to perturbate the whole $4 \times 4$ surface. The wide effect arises from the coupling of $O_2$ to the surface wave functions. In the experimental results [72, 73] such wide effect is not seen and no protrusions around the oxygen regions are met. The wide effect suggests that in modeling of STM of adsorbate molecules even larger simulation cells should be used.

All the constant current images with $I \leq 1 * 10^{-6}$ nA look the same, and there is only a slight $10^{-4}$ Å change in tip height, although the current is decreased roughly. The images show no correspondence to the constant height images, except for the similar depression on the position of the $O_2$ molecule. The constant height and constant current images should be correspondent, because the constant current images are calculated by interpolating from the constant height images. There is obviously a bug in the STM code.

Because of the poor results on constant current images with the $O_2$ adsorbate, the corrugation curves are calculated from constant height images. The corrugation images thus present the tunneling current as a function of tip position. Corrugation curves are received by doing a simple linescan instead of scanning the whole surface. Again, for proper comparison, linescans are scanned in the same two directions for the clean surface and for the one with the adsorbate. The linescans are presented in figure 4.9.

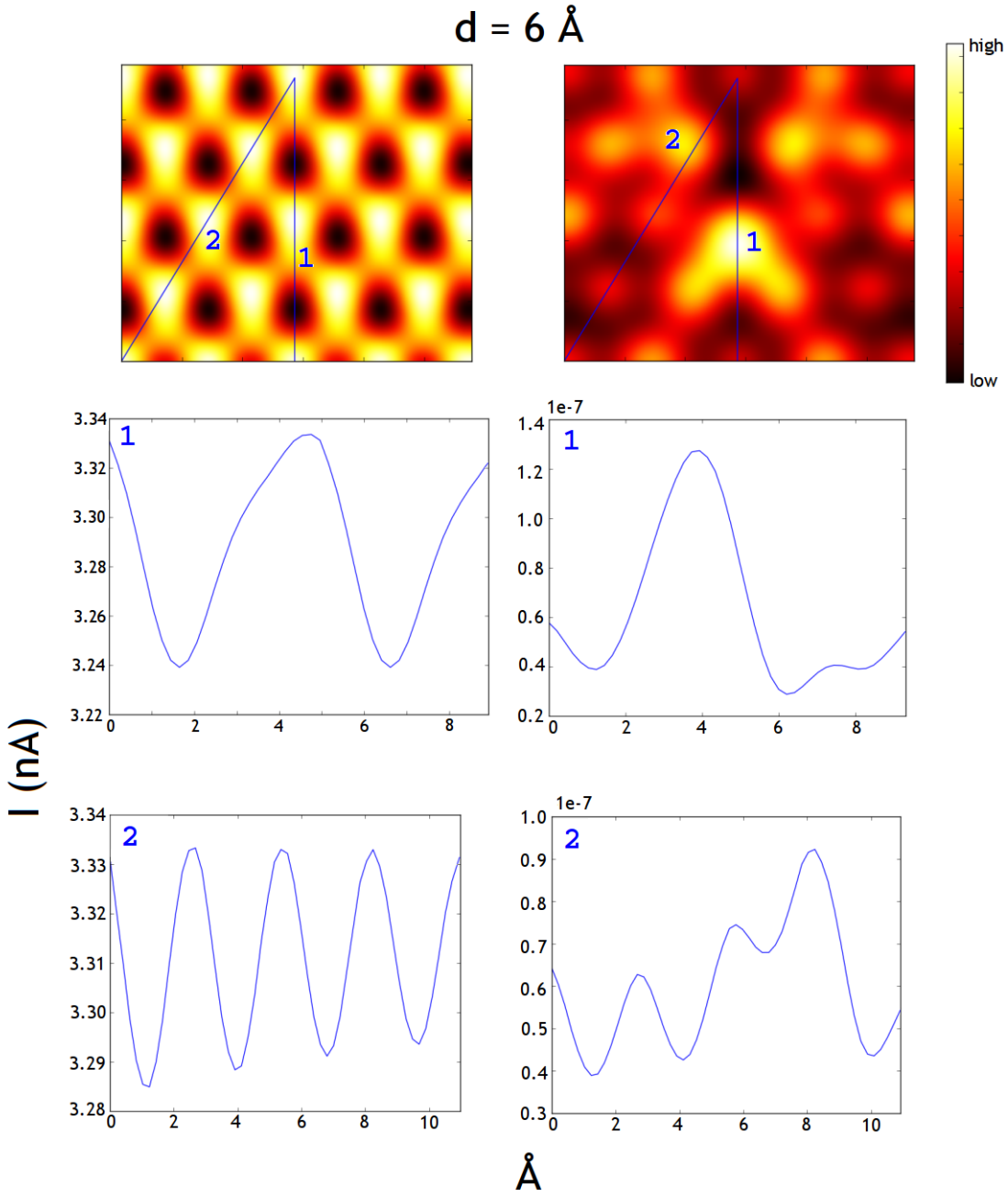


Figure 4.9: Linescans of the a) clean Al(111) surface and b) Al(111) with $O_2$ adsorbate in two directions. The STM image shows the directions of the linescans (1 and 2) presented. The corrugation represents tunneling current's dependency on tip position.

STM images of $H_2$ on Al(111) are not calculated, because the optimization of the system's structure shows that the $H_2$ molecule does not adsorb on the aluminium surface. The optimized structure is illustrated in figure 4.10. The hydrogen molecule stops at distance 3 Å from aluminium surface.

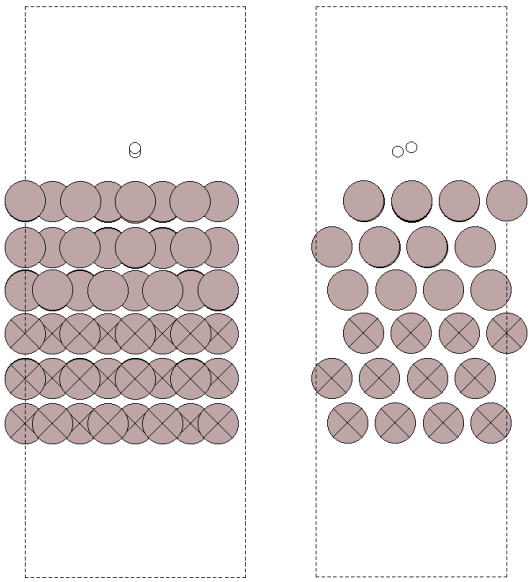

Figure 4.10: The optimized structure of $H_2$ on Al(111) surface. The $H_2$ escapes the surface, instead of adsorbing on it.

## 4.3 Electron transport

Transmission through a molecule trapped between two semi-infinite leads is calculated and imaged. The explored molecules are $H_2$ and $O_2$. The electrodes in both cases consist of Cu(111) surface with the exception that a tip of copper atoms is added to the other lead. The scattering region consists of $4\times4\times4$ copper surfaces on both leads, the copper atom tip attached to the other lead and the molecule trapped between the leads (see pictures 4.11 and 4.12). The projected density of states are calculated and presented with the received transmission results in pictures 4.13 and 4.14.

In the case of $H_2$ adsorbate the transmission is greatest in around energy of 1.5 eV from the Fermi-level. The electronic structure of hydrogen however shows that the energy levels are around 6 eV away from the Fermi level. The energy levels have clearly been shifted and broadened. The calculated picture for projected density of states of the copper surface, shows a peak similar to the transmission peak observed. Also a smaller peak in the vicinity of Fermi level is seen in both images. These peaks are marked in picture 4.13 as "1" and "2". In the projected density of states of $H_2$ no such correspondence is discovered. This implies that the orbitals of hydrogen are not used as transmission channels. Unfortunately the code does not give information of which orbital each line in the PDOS image represents. The code can only tell that they come from *s*- or *d*-orbital.

In the transmission of $O_2$ between copper leads a clear peak is seen on the Fermi level. This fits well with the known electron structure of $O_2$, where there are two

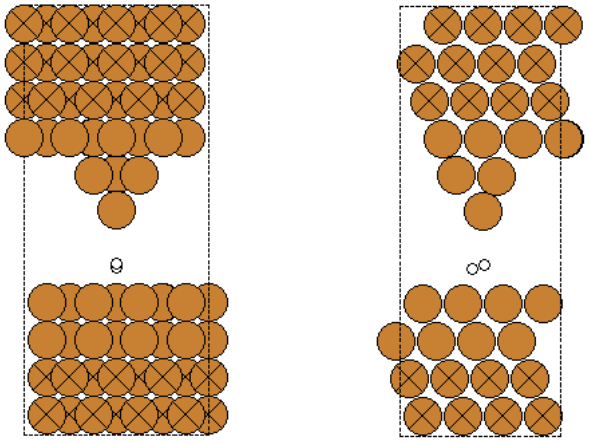

Figure 4.11: Optimized structure of the scattering region of $H_2$ molecule between two Cu(111) leads. The atoms marked with "X" are set still in the optimization.

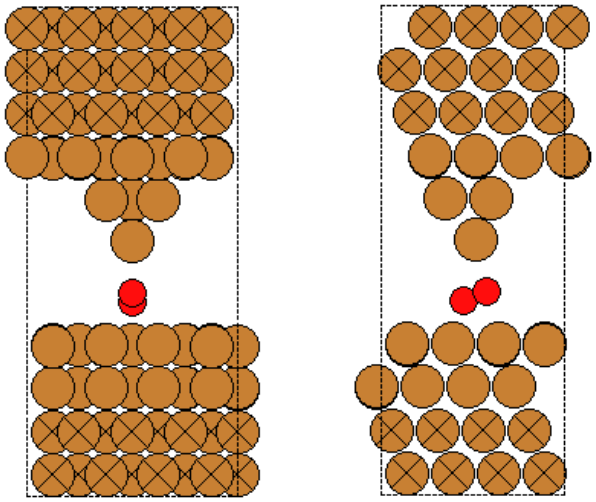

Figure 4.12: Optimized structure of the scattering region of $O_2$ molecule between Cu(111) leads.

degenerate energy levels on the Fermi level. The same peak on Fermi level is seen in the projected density of states of $O_2$ molecular orbitals. The Fermi level peak is marked as "1" in picture 4.14. Other correspondence to $O_2$ molecular orbitals is not seen in the PDOS peaks of $O_2$. The copper surface's PDOS is significantly small compared to other PDOS values calculated, and does not show correspondence to the transmission. The two orbitals of $O_2$ peaked on the Fermi level work clearly as the major tunneling channel.

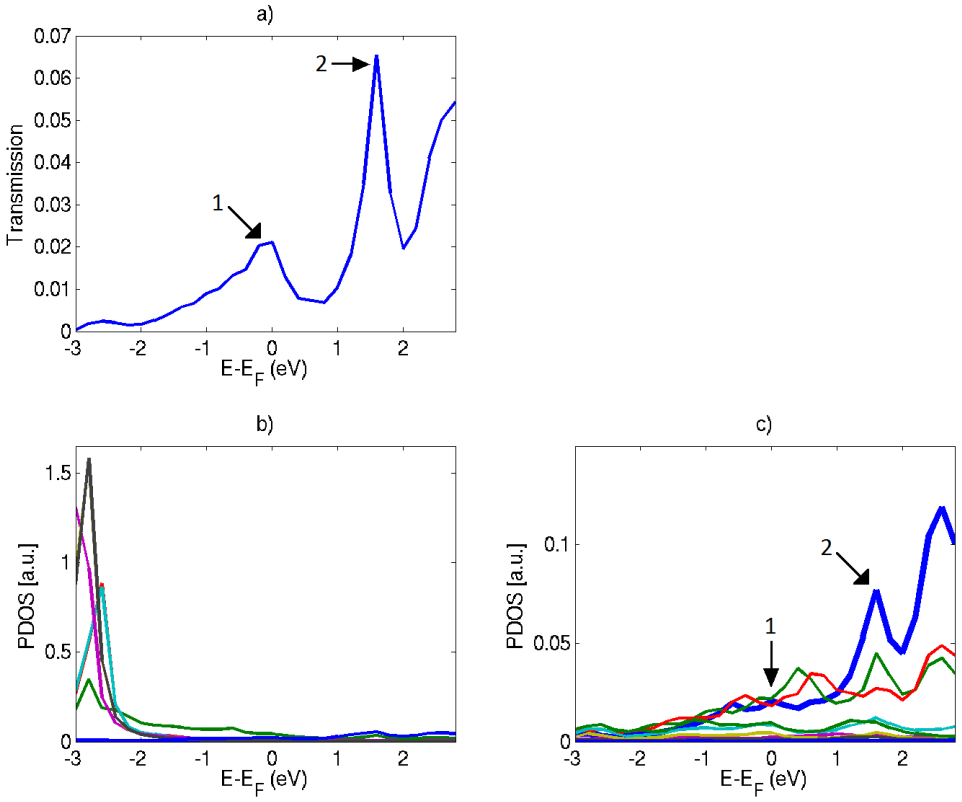


Figure 4.13: a) Transmission through the $H_2$ adsorbate on Cu(111) surface and b) projected density of states of $H_2$ molecular orbitals and c) copper surface.

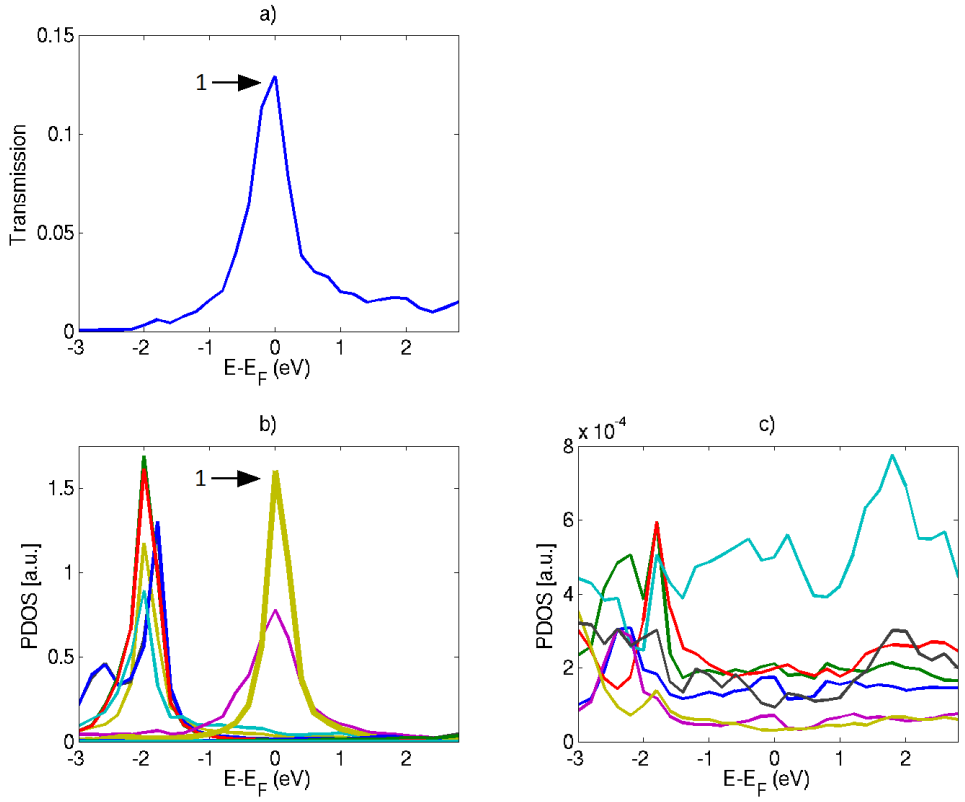


Figure 4.14: a) Transmission through $O_2$ adsorbate on Cu(111) surface and b) projected density of states of $O_2$ molecular orbitals and c) copper surface.

## 4.4 Comments

If there had been time for more simulations, it would have been interesting to see how the chosen molecules act between aluminium leads, as aluminium surface was used in the STM calculations. With the received results no sensible comparison between the transport and STM results can be made.

For future usage of the STM package some serious updating should be made, so it would be possible to simulate any structures and materials. The transport package is functional as it is, and it has potential to be developed into simulation of scanning tunneling spectroscopy. To implement this, the system would have to be separated into two regions as in the STM code, and the boundary conditions should be chosen in a way that would enable moving the regions with respect to one another.

# 5. DISCUSSION AND CONCLUSIONS

The discovery of scanning tunneling microscope, STM, three decades ago was the first method to enable imaging of the atomic structure in real space. Since its invention STM has kept its position as one of the most important tools in modern surface science. In addition it has conquered the world by reproducing numerous applications. Experimenting surfaces with adsorbate molecules has shown that the STM image does not illustrate the geometrical surface, but can show depressions where there geometrically is a protrusion. Understanding the STM images is thus in need of theoretical models and computational simulation.

The goal of this thesis was to test the applicability of grid-based projector augmented wave (GPAW) method to STM and transport calculations. GPAW program package was chosen, because it includes ready packages for studying STM and electron transport with a non equilibrium Green's function (NEGF) method. The particular interest in simulations was to study adsorbate molecules on metal surfaces.

It turned out that the GPAW's STM package is incomplete, and does only apply for certain systems. During the work in progress the GPAW developers announced that the STM code is no longer maintained and it "may or may not work". In principle the theory is implemented, but in practice the code's functionality is dependent on the materials, geometry and chosen LCAO basis. The STM calculations were thus restricted to surfaces that did produce results. Luckily the transport package did not cause any trouble.

Despite the setbacks with the STM package, some successful STM results were received. To get an insight what happens, when an adsorbate is added to the surface, the simulations were carried out to clean surfaces and surfaces with adsorbates. Both constant current and constant height STM images were received to Al(111) and Al(111) with $O_2$ adsorbate. The images and linescans showed that the oxygen molecule is seen as a depression on the surface, although it geometrically is seen as a protrusion. Similar depressions are met in experimental studies of a similar system [72, 73].

Electron transport was studied with a system, where two copper, Cu(111), leads sandwich an $O_2$ or an $H_2$ molecule between them. Comparison of the transmission and projected density of states led to a conclusion that with the $H_2$ molecule the

transmission is through the copper surface, and with $O_2$ molecule, the molecule acts as the tunneling channel. Transmission is most seemingly dependent on the molecule and its electronic structure.

It is concluded that GPAW shows some promising potential in calculation of scanning tunneling microscopy and electron transport. Even though the STM package used in this thesis does not work, GPAW has all the tools for calculation of Green's functions in an atomic orbital basis, and thus enables developing of tailor-made STM and STS applications. The present GPAW's STM package is recommended to use with a bit of caution until it is being updated to work for more than a couple of systems. In the mean time, other promising program packages, such as Nt_STM [34], should be considered for calculational purposes.

All in all, even though the program package did not work as was expected, a few successful results of STM of adsorbate molecules on metal surfaces, and electron transport through different molecules, were received. The thesis succeeds in giving some general results of simulated scanning tunneling microscopy of adsorbate molecules on metal surfaces.

# BIBLIOGRAPHY

[1] G. Binnig, H. Rohrer, Ch. Gerber, and E. Weibel. Surface studies by scanning tunneling microscopy. *Phys. Rev. Lett.*, 49:57–61, Jul 1982.

[2] R. Wiesendanger. *Scanning probe microscopy and spectroscopy: methods and applications*. Cambridge Univ Pr, 1994.

[3] C.F. Quate. Vacuum tunneling: A new technique for microscopy. *Physics Today*, 39:26, 1986.

[4] Y. Kuk and PJ Silverman. Scanning tunneling microscope instrumentation. *Review of scientific instruments*, 60(2):165–180, 1989.

[5] Michael Schmid. Schematic view of an STM. `http://www.iap.tuwien.ac.at/www/surface/stm_gallery/stm_schematic`, 2010. Accessed July 25th, 2012.

[6] Lahti S. Pinta-adsorbaattisyteemien pyyhkäisytunnelointimikroskopian mallintaminen. Diplomityö, Tampereen teknillinen yliopisto, 2009.

[7] G. Binnig and H. Rohrer. In touch with atoms. *Reviews of Modern Physics*, 71(2):324–330, 1999.

[8] DW Pohl, W. Denk, and M. Lanz. Optical stethoscopy: Image recording with resolution $\lambda/20$. *Applied physics letters*, 44(7):651–653, 1984.

[9] G. Binnig, C. F. Quate, and Ch. Gerber. Atomic force microscope. *Phys. Rev. Lett.*, 56:930–933, Mar 1986.

[10] Shozo Suto, Kazuyuki Sakamoto, Takanori Wakita, Chang-Wu Hu, and Atsuo Kasuya. Vibrational properties and charge transfer of $C_{60}$ adsorbed on Si(111)-$(7 \times 7)$ and Si(100)-$(2 \times 1)$ surfaces. *Phys. Rev. B*, 56:7439–7445, Sep 1997.

[11] L. Li, C. Tindall, O. Takaoka, Y. Hasegawa, and T. Sakurai. Structural and vibrational properties of 6H-SiC (0001) surfaces studied using STM/HREELS. *Surface science*, 385(1):60–65, 1997.

[12] M. Hawley, I.D. Raistrick, J.G. Beery, and R.J. Houlton. Growth mechanism of sputtered films of $YBa_2Cu_3O_7$ studied by scanning tunneling microscopy. *Science*, 251(5001):1587–1589, 1991.

[13] Z. Zhang and M.G. Lagally. Atomistic processes in the early stages of thin-film growth. *Science*, 276(5311):377–383, 1997.

[14] U. Dürig, O. Züger, and DW Pohl. Observation of metallic adhesion using the scanning tunneling microscope. *Physical review letters*, 65(3):349–352, 1990.

[15] R. J. Hamers, Ph. Avouris, and F. Bozso. Imaging chemical-bond formation with the scanning tunneling microscope: $NH_3$ dissociation on Si(001). *Phys. Rev. Lett.*, 59:2071–2074, Nov 1987.

[16] P. Avouris, RE Walkup, AR Rossi, HC Akpati, P. Nordlander, T.C. Shen, GC Abeln, and JW Lyding. Breaking individual chemical bonds via STM-induced excitations. *Surface science*, 363(1):368–377, 1996.

[17] RM Overney, E. Meyer, J. Frommer, D. Brodbeck, R. Lüthi, L. Howald, HJ Gintherodt, M. Fujihira, H. Takano, and Y. Gotoh. Friction measurements on phase-separated thin films with a modified atomic force microscope. *Nature*, 359(6391):133–135, 1992.

[18] H. Mizuno, M. Kjellin, N. Nordgren, T. Pettersson, V. Wallqvist, M. Fielden, and M.W. Rutland. Friction measurement between polyester fibres using the fibre probe SPM. *Australian journal of chemistry*, 59(6):390–393, 2006.

[19] B. Bhushan, J.N. Israelachvili, and U. Landman. Nanotribology: friction, wear and lubrication at the atomic scale. *Nature*, 374(6523):607–616, 1995.

[20] D. Sarid. *Scanning force microscopy: with applications to electric, magnetic, and atomic forces*, volume 5. Oxford University Press, USA, 1994.

[21] W.S. Yun, J. Jeffrey, Q. Gu, and H. Park. Ferroelectric properties of individual barium titanate nanowires investigated by scanned probe microscopy. *Nano letters*, 2(5):447–450, 2002.

[22] M.F. Crommie, C.P. Lutz, and D.M. Eigler. Confinement of electrons to quantum corrals on a metal surface. *Science*, 262(5131):218, 1993.

[23] J.A. Stroscio and DM Eigler. Atomic and molecular manipulation with the scanning tunneling microscope. *Science*, 254(5036):1319–1326, 1991.

[24] AS Foster, WA Hofer, and AL Shluger. Quantitative modelling in scanning probe microscopy. *Current Opinion in Solid State and Materials Science*, 5(5):427–434, 2001.

[25] G. Binnig and H. Rohrer. Scanning tunneling microscopy. *Surface Science*, 126(1):236–244, 1983.

[26] Joseph A. Stroscio, R. M. Feenstra, and A. P. Fein. Electronic structure of the Si(111) 2×1 surface by scanning-tunneling microscopy. *Phys. Rev. Lett.*, 57:2579–2582, Nov 1986.

[27] L. Bartels, G. Meyer, and K.H. Rieder. The evolution of CO adsorption on Cu (111) as studied with bare and CO-functionalized scanning tunneling tips. *Surface science*, 432(3):L621–L626, 1999.

[28] Werner A. Hofer, Adam S. Foster, and Alexander L. Shluger. Theories of scanning probe microscopes at the atomic scale. *Rev. Mod. Phys.*, 75:1287–1331, Oct 2003.

[29] GAD Briggs and AJ Fisher. STM experiment and atomistic modelling hand in hand: individual molecules on semiconductor surfaces. *Surface science reports*, 33(1):1–81, 1999.

[30] J. Bardeen. Tunneling from a many-particle point of view. *Physical Review Letters*, 6:57–59, 1961.

[31] J. Tersoff and DR Hamann. Theory of the scanning tunneling microscope. *Physical Review B*, 31(2):805–813, 1985.

[32] M. Büttiker, Y. Imry, R. Landauer, and S. Pinhas. Generalized many-channel conductance formula with application to small rings. *Phys. Rev. B*, 31:6207–6215, May 1985.

[33] Yigal Meir and Ned S. Wingreen. Landauer formula for the current through an interacting electron region. *Phys. Rev. Lett.*, 68:2512–2515, Apr 1992.

[34] M. Magoga, F. Archambault, and J.I. Cerdá. Nt_STM: A step forward in scanning tunneling microscopy (STM) simulations. *Computer Physics Communications*, 183(6):1246–1249, 2012.

[35] T.N. Todorov, GAD Briggs, and AP Sutton. Elastic quantum transport through small structures. *Journal of Physics: Condensed Matter*, 5:2389, 1993.

[36] JB Pendry, AB Prêtre, and BCH Krutzen. Theory of the scanning tunnelling microscope. *Journal of Physics: Condensed Matter*, 3:4313–4321, 1991.

[37] P.A. Tipler and R.A. Llewellyn. *Modern physics*. WH Freeman, fifth edition, 2003.

[38] S. Gasiorowicz. *Quantum physics*. John Wiley & Sons, third edition, 2003.

[39] H.B. Michaelson. The work function of the elements and its periodicity. *Journal of Applied Physics*, 48(11):4729–4733, 1977.

[40] Yigal Meir, Ned S. Wingreen, and Patrick A. Lee. Transport through a strongly interacting electron system: Theory of periodic conductance oscillations. *Phys. Rev. Lett.*, 66:3048–3051, Jun 1991.

[41] N.E. Cusack and D.L. Stein. The physics of structurally disordered matter: an introduction. *Physics Today*, 41:110, 1988.

[42] G. Rickayzen. *Green's functions and condensed matter*. Academic Press, Inc., New York, NY, 1980.

[43] G.B. Arfken, H.J. Weber, and F.E. Harris. *Mathematical Methods for Physicists: A Comprehensive Guide*. Academic press, 2012.

[44] P.A.M. Dirac. The principles of quantum mechanics. *The International Series of Monographs on Physics*, 1, 1947.

[45] J.M. Ziman. *Elements of advanced quantum theory*. Cambridge Univ Pr, 1975.

[46] Mads Brandbyge, José-Luis Mozos, Pablo Ordejón, Jeremy Taylor, and Kurt Stokbro. Density-functional method for nonequilibrium electron transport. *Phys. Rev. B*, 65:165401, Mar 2002.

[47] L.P. Kadanoff and G. Baym. *Quantum statistical mechanics: Green's function methods in equilibrium and nonequilibrium problems*. Benjamin, 1962.

[48] M. Paulsson. Non equilibrium green's functions for dummies: Introduction to the one particle NEGF equations. *Arxiv preprint cond-mat/0210519*, 2002.

[49] P. Hohenberg and W. Kohn. Inhomogeneous electron gas. *Phys. Rev.*, 136:B864–B871, Nov 1964.

[50] W. Kohn and L. J. Sham. Self-consistent equations including exchange and correlation effects. *Phys. Rev.*, 140:A1133–A1138, Nov 1965.

[51] J. J. Mortensen, L. B. Hansen, and K. W. Jacobsen. Real-space grid implementation of the projector augmented wave method. *Phys. Rev. B*, 71:035109, Jan 2005.

[52] P.W. Atkins, R.S. Friedman, and Inc NetLibrary. *Molecular quantum mechanics*, volume 3. Oxford University Press Oxford, 1997.

[53] G. van Rossum and J. de Boer. Interactively testing remote servers using the Python programming language. *CWI Quarterly*, 4(4):283–303, 1991.

[54] P. E. Blöchl. Projector augmented-wave method. *Phys. Rev. B*, 50:17953–17979, Dec 1994.

[55] K.S. Thygesen and A. Rubio. Non-equilibrium GW approach to quantum transport in nano-scale contacts. *Arxiv preprint cond-mat/0609223*, 2006.

[56] J. Enkovaara, C. Rostgaard, J.J. Mortensen, J. Chen, M. Dułak, L. Ferrighi, J. Gavnholt, C. Glinsvad, V. Haikola, HA Hansen, et al. Electronic structure calculations with GPAW: a real-space implementation of the projector augmented-wave method. *Journal of Physics: Condensed Matter*, 22:253202, 2010.

[57] A.H. Larsen, M. Vanin, J.J. Mortensen, K.S. Thygesen, and K.W. Jacobsen. Localized atomic basis set in the projector augmented wave method. *Physical Review B*, 80(19):195112, 2009.

[58] C. Rostgaard. The projector augmented-wave method. *Arxiv preprint arXiv:0910.1921*, 2009.

[59] JC Slater. Wave functions in a periodic potential. *Physical Review*, 51(10):846, 1937.

[60] C. Herring. A new method for calculating wave functions in crystals. *Physical Review*, 57(12):1169, 1940.

[61] P.E. Blöchl, J. Kästner, and C.J. Först. Electronic structure methods: Augmented waves, pseudopotentials and the projector augmented wave method. *Handbook of Materials Modeling*, pages 93–119, 2005.

[62] S. R. Bahn and K. W. Jacobsen. An object-oriented scripting interface to a legacy electronic structure code. *Comput. Sci. Eng.*, 4(3):56–66, 2002.

[63] K. W. Jacobsen, J. K. Norskov, and M. J. Puska. Interatomic interactions in the effective-medium theory. *Phys. Rev. B*, 35:7423–7442, May 1987.

[64] H. Hakkinen and M. Manninen. The effective-medium theory beyond the nearest-neighbour interaction. *Journal of Physics: Condensed Matter*, 1:9765, 1989.

[65] H. Lin, J.M.C. Rauba, K.S. Thygesen, K.W. Jacobsen, M.Y. Simmons, and W.A. Hofer. First-principles modelling of scanning tunneling microscopy using non-equilibrium Green's functions. *Frontiers of Physics in China*, 5(4):369–379, 2010.

[66] J.M.C. Rauba. Scanning tunneling microscopy simulations using non-equilibrium green functions. Master's thesis, Technical University of Denmark, 2009.

[67] CAMd et al. STM-simulations using Green's functions. `https://wiki.fysik.dtu.dk/gpaw/tutorials/negfstm/negfstm.html?highlight=stm%20simulations`, 2012. Accessed July 23rd, 2012.

[68] David R. Lide. Characteristic bond lengths in free molecules. In *CRC Handbook of Chemistry and Physics*. CRC Press / Taylor and Francis, 92nd edition, 2012. Internet version.

[69] L. Laaksonen. *gOpenMol 2.32*, 2002. Center for Scientific Computing, Espoo, Finland.

[70] Christian Glinsvad. [gpaw-users] An error occurs when performing STM simulation using GPAW. `https://listserv.fysik.dtu.dk/pipermail/gpaw-users/2010-July/000227.html`, 2010. Accessed July 26th, 2012.

[71] Christian Glinsvad. [gpaw-users] An error occurs when performing STM simulation using GPAW. `https://listserv.fysik.dtu.dk/pipermail/gpaw-users/2010-July/000236.html`, 2010. Accessed July 26th, 2012.

[72] M. Schmid, G. Leonardelli, R. Tscheließnig, A. Biedermann, and P. Varga. Oxygen adsorption on Al (111): low transient mobility. *Surface science*, 478(3):L355–L362, 2001.

[73] J. Wintterlin, H. Brune, H. Höfer, and RJ Behm. Atomic scale characterization of oxygen adsorbates on Al (111) by scanning tunneling microscopy. *Applied Physics A: Materials Science & Processing*, 47(1):99–102, 1988.

# A. APPENDIX

This appendix section represents GPAW-scripts used in this thesis. The scripts are presented only for a single geometric structure, because the script is the same for other structures. The only thing changing between structures is the definition of the initial geometric structure, and in STM code the principal layer size changes when changing between fcc(111) and fcc(100). All scripts are commented, '#' on a line denotes that text after that is a comment.

## A.1 Electronic structure scripts

Electronic structure scripts calculate the electronic structure of a molecule. The script is handed an initial geometric structure, which is optimized, and as a result the electronic structure, that is the wave functions and energy levels, are obtained. GPAW calculator is given the same parameters as in transport calculations.

```
from ase.all import *
from ase.optimize import QuasiNewton
from gpaw import GPAW, Mixer, FermiDirac

basename = 'o2'

# Distance between O2-atoms, i.e. the initial bond length
d = 1.21

# Initial structure
atoms = Atoms([Atom('O', (0,0,0)), Atom('O', (0,0,d))])

atoms.center(vacuum=3.0)

# Define the calculator
calc = GPAW(h=0.3,
            xc='PBE',
            basis='szp(dzp)',
            occupations=FermiDirac(width=0.4),
            mode='lcao',
```

```
            txt=basename+'opt.txt',
            mixer=Mixer(0.05, 10, weight=100.0),
            convergence={'energy': 0.05,  # eV / electron
                         'density': 1.0e-2,
                         'eigenstates': 4.0e-3  # eV^2 / electron
                         },
            usesymm=None)

atoms.set_calculator(calc)

# Optimizer defined, here QuasiNewton is the optimizer.
opt = QuasiNewton(atoms, trajectory='o2opt.traj')
opt.run(fmax = 0.05) # Optimize structure until force < fmax

atoms.write(basename+'.xyz')
calc.write(basename+'.gpw', mode='all')

#Wave functions
nbands = calc.get_number_of_bands()

for band in range(nbands):
    wf = calc.get_pseudo_wave_function(band=band)

    #Wave functions are saved to their own plt-files
    fname = basename+'_'+'%d' %(band)+'.plt'
    print 'writing wf', band, 'to file', fname
    write(fname, atoms, data=wf)
```

## A.2 STM scripts

For STM calculations, two scripts must be used. The first one defines the STM tip and surface, and calculates Hamiltonians and overlap matrices, $H$ and $S$. The second one calculates the Green's functions and does the actual STM calculations and images. The second part can be done in constant current or constant height mode, for which there are separate scripts.

### A.2.1 Defining the tip and surface

The script defines the STM tip and STM surface. Initial geometric structure for the surface (fcc(111) or fcc(100)) is received directly from ASE. The tip is a hydrogen

atom chain. In the presented script, an adsorbate molecule is added. For clean surfaces the adding of the adsorbate is omitted easily by deleting a couple of lines of the code.

```
from ase.all import *
from ase import Atoms, Atom
from gpaw import GPAW, Mixer
from ase.lattice.surface import fcc111, add_adsorbate
from gpaw.transport.jstm import dump_hs, dump_lead_hs
from ase.constraints import FixAtoms, FixBondLength
from ase.optimize import QuasiNewton

calc = GPAW(h=0.2,
            mixer=Mixer(0.03, 5, weight=140.0),
            width=0.1,
            mode='lcao',
            basis='szp(dzp)',
            txt='dumphs.txt',
            usesymm=False)

# surface calculation
a = 4.0
srf = fcc111('Al', size=(4, 4, 6), orthogonal = True)

# Add adsorbate
# O_2 bond length
o = 1.21
adsorbate = Atoms('O2', [(0,0,0),(0,o,0)])
add_adsorbate(srf, adsorbate, 2.0,
              position=(srf.positions[-6][0], srf.positions[-6][1]))

srf.pbc=(1,1,0)
srf.center(axis=2, vacuum=8.0)

# Movement of tree top layers of surface
# and O_2's bond length constrained.
c = FixAtoms(mask=[a.index < 48 for a in srf])
b = FixBondLength(96,97)
srf.set_constraint([b,c])
```

```
srf.set_calculator(calc)

opt = QuasiNewton(srf, trajectory='optAlO2.traj')
opt.run(fmax=0.05)

srf.get_potential_energy()
calc.write('srf')

# Dump overlap matrix and Hamiltonian matrix to the local directory.
# Here the keyword 'cvl' refers  to the number of basis functions
# in the convergence layer, i.e. for the present system three atomic
# layers are used.
dump_hs(calc, 'srf', region='surface', cvl=4*4*3*9)

# tip calculation
a = 0.75 # lattice constant
tip = Atoms('H12', pbc=(1, 1, 0), cell=[5, 5, 12 * a + 7])
tip.positions[:,2] = [i * a for i in range(12)]
tip.positions[:] += (tip.cell / 2.0)[0, :] + (tip.cell / 2.0)[1, :]
tip.translate([0, 0, 6])

tip.set_calculator(calc)
tip.get_potential_energy()
calc.write('tip')
dump_hs(calc, 'tip', region='tip', cvl=4)

# The k-points changed for the lead calculation
calc.set(kpts=(1, 1, 7))

# surface principal layer calculation
srf_p = fcc111('Al', size=(4, 4, 3), orthogonal = True)
srf_p.pbc = (1, 1, 1)

srf_p.set_calculator(calc)
srf_p.get_potential_energy()
dump_lead_hs(calc, 'srf_p') # dump overlap and hamiltonian matrix

# tip principal layer calculation
tip_p = Atoms('H4', pbc=(1,1,1), cell=[5, 5, 4*a])
```

```
tip_p.positions[:,2] = [i * a for i in range(4)]
tip_p.positions[:] += ((tip_p.cell / 2.0)[0, :] +
                       (tip_p.cell / 2.0)[1, :])
tip_p.set_calculator(calc)
tip_p.get_potential_energy()
dump_lead_hs(calc, 'tip_p') # dump overlap and hamiltonian matrix
```

### A.2.2 Constant height images

Constant height images are calculated with the following script. The script also produces linescan images. In the script the tip height from the surface is defined in parameter `dmin`. The images calculated are saved in png-format.

```
import pickle
from gpaw import GPAW
from gpaw.transport.jstm import STM
from ase.io import write
import matplotlib
matplotlib.use('Agg')
import pylab

basename = 'd6Al02'
form = '.png'

# tip:
tip = GPAW('tip', txt=None)
h1, s1 = pickle.load(open('tip_hs.pckl')) # h ja s matrices
h10, s10 = pickle.load(open('tip_p_hs.pckl')) # for principal layer

# surface:
srf = GPAW('srf', txt=None)
h2, s2 = pickle.load(open('srf_hs.pckl'))
h20, s20 = pickle.load(open('srf_p_hs.pckl'))

#STM calculator:
stm = STM(tip, srf,
          hs1=(h1[0], s1[0]),   # tip
          hs10=(h10[0], s10[0]),# tip's principal layer
          hs2=(h2[0], s2[0]),   # surface
          hs20=(h20[0], s20[0]),# surface's principal layer
          bias = 0.05,          # bias voltage
```

```
          de = 0.05/7.,         # spacing of the energy grid at which
                                # Green's functions are evaluated
          logfile='scan.log')

stm.set(dmin=6) # dmin is the distance between the tip and surface

# Initialization of the STM calculator
stm.initialize()

# STM scan
stm.scan()

# Linescan
stm.linescan([[0, 0],[25, 43.3]])

# Plot the current map and the linescan
stm.plot(label='I[nA]')

# Save figures to file.
pylab.savefig(basename+'linescan'+form)
pylab.close()
pylab.savefig(basename+'surface'+form)
```

### A.2.3 Constant current images

Constant current images are obtained by interpolation. The script calculates constant height images in specified region `zmin..zmax`, and the constant current image is calculated by interpolating between constant height images. The images are saved in png-format.

```
import pickle
from gpaw import GPAW
from gpaw.transport.jstm import STM
from ase.io import write
import matplotlib
matplotlib.use('Agg')
import pylab

# Tip:
tip = GPAW('tip', txt=None)
h1, s1 = pickle.load(open('tip_hs.pckl')) # h ja s matrices
```

```
h10, s10 = pickle.load(open('tip_p_hs.pckl')) # Principal layer's h & s

# Surface:
srf = GPAW('srf', txt=None)
h2, s2 = pickle.load(open('srf_hs.pckl'))
h20, s20 = pickle.load(open('srf_p_hs.pckl'))

# STM calculator:
stm = STM(tip, srf,
          hs1=(h1[0], s1[0]),
          hs10=(h10[0], s10[0]),
          hs2=(h2[0], s2[0]),
          hs20=(h20[0], s20[0]),
          bias = 0.5,
          de = 0.5/7.,
          logfile='scan.log')

stm.scan3d(zmin=5.0, zmax=7.0, filename='scan3d')

current = 1.5e-8

stm.read_scans_from_file('scan3d')
stm.get_constant_current_image(current)

# Plot the constant current STM image
stm.plot()

pylab.savefig(basename+'surface'+form)
```

## A.3 Transport scripts

Electron transport is as well calculated in two parts. The first script calculates the Hamiltonian overlap matrices, and the second calculates transmission and projected density of states using the received infromation. The structure of the transport system differs from STM system, so the defining of the geometric structure is not quite simple.

### A.3.1 Calculating the Hamiltonian and overlap matrices

This script includes a long section of defining the geometric structure of the scattering region. The left lead is constructed by copying a number of layers from the

scattering region's left side and the right lead is assumed identical.

```
from ase import Atoms, Atom
from gpaw import GPAW, Mixer, FermiDirac
from gpaw.lcao.tools import remove_pbc, get_lcao_hamiltonian
from gpaw lcao.tools import get_lead_lcao_hamiltonian
from ase.lattice.surface import fcc111, add_adsorbate
import cPickle as pickle

a = 2.41 # Cu binding length
b = 0.90 # H2 binding length
c = 1.70 # Cu-H binding length
L = (7.00/2)*4 # width of unit cell
ncux = 4 # number of Cu-atoms in x-direction
ncuy = 4

######################
# Scattering region #
######################

# Setup the Atoms for the scattering region.

# srf is the slab below the sample
srf = fcc111('Cu', size=(ncux, ncuy, 4), orthogonal = True)
srf.pbc=(1,1,1)

xcell = srf.cell[0][0]
ycell = srf.cell[1][1]

xcell1 = 5.105/2*ncux
ycell1 = 4.4213/2*ncuy

# Middle of the cell in x- and y-directions.
xcell2 = xcell1/2
ycell2 = ycell1/2

# The created srf is copied to the other side of the sample.
srf1 = srf.copy();

# mxsrf is the maximum z-component of the surface.
```

```
mxsrf = max(srf.positions[:,2])

# The copy is moved up and to the side to match with next slab layer.
# The copied surface srf1 moves 9 Angstroms from srf.
shift = 9.0+mxsrf
srf1.positions[:,2] += shift
srf.positions[:,0] += xcell1/ncux/2
srf.positions[:,1] += ycell1/ncuy/2

# The distance between the slabs.
mxsrf = max(srf.positions[:,2])
mnsrf = min(srf.positions[:,2])
mnsrf1 = min(srf1.positions[:,2])
mxsrf1 = max(srf1.positions[:,2])

# Midpoint of the region between the slabs in z-direction.
meanp = 0.5*(mxsrf1+mnsrf)

# Size of the scattering region in z-direction
boz= abs(mxsrf1-mnsrf)

# Size of one lead in z-direction
bozlead=abs(mxsrf-mnsrf)

# dlay is the distance between the layers of the slab
dlay = abs(srf.positions[0][2]-srf.positions[4][2])
d = 1.10
tipz = mnsrf1 - 1.5 -2

# Defining of the molecule and tip.
molecule = Atoms('2H', positions=[(xcell2, ycell2, mxsrf+c),
                                  (xcell2, ycell2, mxsrf+c+b)])
tip = Atoms('4Cu', positions= [(xcell2, ycell2, tipz),
                               (xcell2+1.382, ycell2-0.834,
                                tipz+2.024),
                               (xcell2-1.382, ycell2-0.834,
                                tipz+2.024),
                               (xcell2, ycell2+1.562,
                                tipz+2.024)])
```

```
slab = srf
slab += molecule
slab += tip
slab +=srf1
slab.positions[:,2] + boz/2
slab.set_cell([xcell1,ycell1,boz+dlay])
slab.center()

slab.set_pbc([1,1,1])

# The structure is optimized.
from ase.constraints import FixAtoms, FixedPlane
from ase.calculators.emt import EMT
from ase.optimize import QuasiNewton

# The position of some atoms is fixed.
mask = (slab.positions[:, 2] > boz-5.0)
mask += (slab.positions[:, 2] < 5.0)
fixlayers = FixAtoms(mask=mask)
slab.set_constraint(fixlayers)

# Use EMT potential in the relaxation calculation:
slab.set_calculator(EMT())

relax = QuasiNewton(slab,trajectory='structure.traj')
relax.run(fmax=0.05)

# Attach a GPAW calculator
calc = GPAW(h=0.3,
            xc='PBE',
            basis='szp(dzp)',
            occupations=FermiDirac(width=0.4),
            kpts=(2, 2, 1),
            mode='lcao',
            txt='cu_h2_lcao_scat.txt',
            mixer=Mixer(0.05, 10, weight=100.0),
            convergence={'energy': 0.05,  # eV / electron
                         'density': 1.0e-2,
```

```
                        'eigenstates': 4.0e-3  # eV^2 / electron
                        },
            usesymm=None)

slab.set_calculator(calc)
slab.get_potential_energy() # Converge everything!
Ef = slab.calc.get_fermi_level()

H_skMM, S_kMM = get_lcao_hamiltonian(calc)
if mpi.rank==0:
    for H_kMM in H_skMM:
        H_kMM  -= Ef * S_kMM
        for H_MM, S_MM in zip(H_kMM, S_kMM):
            remove_pbc(slab, H_MM, S_MM, 2)
    # Dump the Hamiltonian and scattering matrix to a pickle file
    pickle.dump((H_skMM, S_kMM), open('scat_hs.pickle', 'wb'), 2)

calc.write('cuh2.gpw', 'all')

########################
# Left principal layer #
########################

# Use four Cu atoms in the lead, so only take those from before
leadth = 3
bozlead = leadth*abs(srf.positions[0][2]-
                     srf.positions[ncux*ncuy][2])
# Copy layers from the scattering region's side to construct
# the principal layer.
slab = slab[:leadth*ncux*ncuy].copy()
slab.set_cell([xcell1, ycell1, bozlead])

# Attach a GPAW calculator
calc = GPAW(h=0.3,
            xc='PBE',
            basis='szp(dzp)',
            occupations=FermiDirac(width=0.4),
            kpts=(2, 2, 2),
            mode='lcao',
```

```
            txt='cu_h2_lcao_llead.txt',
            mixer=Mixer(0.05, 5, weight=100.0),
            convergence={'energy': 0.05,  # eV / electron
                         'density': 1.0e-2,
                         'eigenstates': 4.0e-3  # eV^2 / electron
                         },
            usesymm=None)
slab.set_calculator(calc)

slab.get_potential_energy() # Converge everything!
Ef = slab.calc.get_fermi_level()

ibz2d_k, weight2d_k, H_skMM, S_kMM = get_lead_lcao_hamiltonian(calc)
if mpi.rank==0:
    for H_kMM in H_skMM:
        H_kMM  -= Ef * S_kMM
    # Dump the hamiltonian and overlap matrix to pickle file.
    pickle.dump((H_skMM, S_kMM), open('lead1_hs.pickle', 'wb'), 2)
    # Right principal layer is identical:
    pickle.dump((H_skMM, S_kMM), open('lead2_hs.pickle', 'wb'), 2)
```

### A.3.2 Calculation of transmission and PDOS

The actual transport calculation is done with the following script. The script gives transmission coefficient $\mathcal{T}(E)$ and projected density of states $\rho(E)$.

```
from ase.transport.calculators import TransportCalculator
import numpy as np
import pickle

import matplotlib
matplotlib.use('Agg')
import pylab
import pylab as plt

# Size of the slab is ncux*ncuy*ncuz
ncux=4
ncuy=4 # horizontal size of the slab
ncuz=4
```

```
# Determine the basis functions of the two Hydrogen atoms
# and subdiagonalize
Cu_N = ncux*ncuy*ncuz # Number of Cu atoms on each side
                      # in the scattering region
H_N = 2
Cu_nbf = 9 # number of bf per Cu atom (basis=szp)
H_nbf = 4  # number of bf per H atom (basis=szp)
H_nbf = H_N*H_nbf
bf_H1 = Cu_nbf * Cu_N
bfs = range(bf_H1, bf_H1 + H_nbf + Cu_nbf)

energies=np.arange(-3, 3, 0.2)
T = np.zeros(len(energies))
pdos_ne = np.zeros((len(bfs),len(energies)))

# Read in the hamiltonians and overlap matrices
H, S = pickle.load(file('scat_hs.pickle'))
H1, S1 = pickle.load(file('lead1_hs.pickle'))
H2, S2 = pickle.load(file('lead2_hs.pickle'))

# k-points
nkpts = H.shape[1]

s=0

for k in range(0,nkpts):
      H_k= H[s, k]
      S_k= S[k]

      H1_k= H1[s, k]
      S1_k= S1[k]
      H2_k= H2[s, k]
      S2_k= S2[k]

      # eta is broadening of scattering levels
      # eta1 is broadening of lead 1 and eta2 of lead 2.
      tcalc = TransportCalculator(h=H_k, h1=H1_k, h2=H2_k,
                                  s=S_k, s1=S1_k, s2=S2_k,
                                  align_bf=1,
```

```
                                    eta=0.1,
                                    eta1=0.2,
                                    eta2=0.2)

      # energies is the energy grid on which the transport
      # properties are determined
      tcalc.set(energies=np.arange(-3, 3, 0.2))
      T_k = tcalc.get_transmission()
      T +=T_k

      h_rot, s_rot, eps_n, vec_jn = tcalc.subdiagonalize_bfs(bfs)

      # Switch to the rotated basis set
      tcalc.set(h=h_rot, s=s_rot)

      # Projected density of states is received:
      tcalc.set(pdos=bfs)

      pdos_ne_k = tcalc.get_pdos()
      pdos_ne += pdos_ne_k

T = T/nkpts
pdos_ne=pdos_ne/nkpts

# Plot the transmission function
pylab.plot(tcalc.energies, T)
pylab.title('Transmission function')
plt.savefig('transmission')
plt.clf()

# Plot the projected density of states of the hydrogen molecule
for ior in range(0,H_nbf):
    pylab.plot(tcalc.energies, pdos_ne[ior], label='s-orbital')
    # The information is saved to .txt format
    f = open('pdos_H_'+str(ior)+'.txt', 'w');
    print >>f, tcalc.energies, pdos_ne[ior]
    f.close()

pylab.title('Projected density of states')
```

```
plt.savefig('pdos_H')
plt.clf()

# Projected density of states of copper surface with H_2 plotted:
for ior in range(H_nbf,H_nbf+Cu_nbf):
    pylab.plot(tcalc.energies, pdos_ne[ior], label='s/d-orbital')
    f = open('pdos_Cu_'+str(ior)+'.txt', 'w');
    print >>f, tcalc.energies, pdos_ne[ior]
    f.close()

pylab.title('Projected density of states')
pylab.legend()
plt.savefig('pdos_Cu')
plt.clf()
```